

OPEN ACCESS

EDITED BY
Dawei Wang,
RWTH Aachen University, Germany

REVIEWED BY
Chao Xing,
Harbin Institute of Technology, China
Augusto Cannone Falchetto,
University of Padua, Italy
Marco Bruno,
University of Bologna, Italy

Jie Ji, ⊠ jijie@bucea.edu.cn
Pengfei Li,

*CORRESPONDENCE

☑ lipengfei3060@163.com

RECEIVED 31 May 2025
REVISED 13 September 2025
ACCEPTED 16 September 2025
PUBLISHED 25 November 2025

CITATION

Wang Z, Wang Z, Sha C, Guo S, Zheng W, Cao H, Shan X, Cao G, Ji J and Li P (2025) Conduct an advanced numerical simulation investigation on the rutting performance of coal liquefaction residue asphalt mixture. *Front. Mater.* 12:1638678.

COPYRIGHT

© 2025 Wang, Wang, Sha, Guo, Zheng, Cao, Shan, Cao, Ji and Li. This is an open-access article distributed under the terms of the Creative Commons Attribution License (CC BY). The use, distribution or reproduction in other forums is permitted, provided the original author(s) and the copyright owner(s) are credited and that the original publication in this journal is cited, in accordance with accepted academic practice. No use, distribution or reproduction is permitted which does not comply with these terms.

Conduct an advanced numerical simulation investigation on the rutting performance of coal liquefaction residue asphalt mixture

Zhe Wang^{1,2}, Zhen Wang¹, Chuan Sha¹, Shuangfeng Guo^{2,3}, Wenhua Zheng⁴, Hongbo Cao¹, Xiaowei Shan¹, Guoqing Cao⁵, Jie Ji⁴* and Pengfei Li⁶*

¹Beijing Municipal Road and Bridge Building Material Group Co. Ltd., Beijing, China, ²Chongqing University Industrial Technology Research Institute, Chongqing, China, ³College of Transportation Engineering, Nanjing Tech University, Nanjing, Jiangsu, China, ⁴School of Civil and Transportation Engineering, Beijing University of Civil Engineering and Architecture, Beijing, China, ⁵Qingdao NO1 Municipal Engineering Co., Ltd., Qingdao, Shandong, China, ⁶Beijing Xinqiao Technology Development Co., Ltd., Beijing, China

Coal liquefaction residue (CLR), a byproduct of coal-to-liquid technology known to adversely affect the ecological environment and human health, was investigated in this study for its influence on the rutting resistance of asphalt mixtures. The research employed the discrete element method in PFC2D to develop a rutting model, analyzing mixture behavior under varying temperatures and loads. CLR was used to replace fine aggregate volumetrically, with particular focus on particles ranging from 0 to 4.75 mm. Macroscopic rutting behavior was evaluated by examining fine particle displacement and force chain distribution. Results revealed that rutting development follows a power-function growth pattern, divided into three stages: 0-10 minutes, 10-20 minutes, and 20-60 minutes, with the initial 20 minutes being critical for rut formation. Particles exhibited strong self-organization adaptability, reducing stress concentration at rut initiation. During rutting evolution, particles sized 0.6-2.36 mm contributed significantly to deformation, while smaller particles (1.18-2.36 mm) were more prone to passive displacement due to compression and collision with larger particles (2.36-4.75 mm). In asphalt mortar with higher adhesive strength, however, the 0.6-1.18 mm particles were more extensively coated by larger ones, resulting in reduced displacement compared to the 1.18-2.36 mm fraction. The 2.36-4.75 mm particles served as a macroscopic skeleton, bearing and transmitting contact forces. Numerical simulations confirmed the rationality of replacing the 1.18-2.36 mm and 2.36-4.75 mm particles with indirect CLR of single particle sizes, and the 0.6-1.18 mm and 1.18-2.36 mm particles with direct CLR of single particle sizes. It was concluded that direct CLR significantly

enhances the high-temperature performance of asphalt mixtures compared to indirect CLR, which aligns with macroscopic rutting test outcomes.

KEYWORDS

road engineering, coal liquefaction residue, asphalt mixture, rutting behavior, numerical simulation

1 Introduction

China's energy structure remains heavily reliant on coal, which accounts for approximately 70% of the primary energy supply (Wang Bing et al., 2022). While coal liquefaction technologies (direct and indirect processes) offer a cleaner approach to coal utilization (Ji et al., 2023; WANG et al., 2020), they generate substantial byproducts—approximately 30% of feedstock coal is converted into residues (DCLR and ICLR). Indirect coal liquefaction residue (ICLR) exhibits promising potential as an aggregate due to its gravel-like density (2.4–2.8 g/cm³) and high thermal stability (deformation temperature >600 °C) (LIU et al., 2016). In contrast, direct coal liquefaction residue (DCLR) contains 20%–40% asphaltenes and 20%–30% heavy oils, making it a superior candidate for asphalt modification compared to conventional modifiers (Gu et al., 2006).

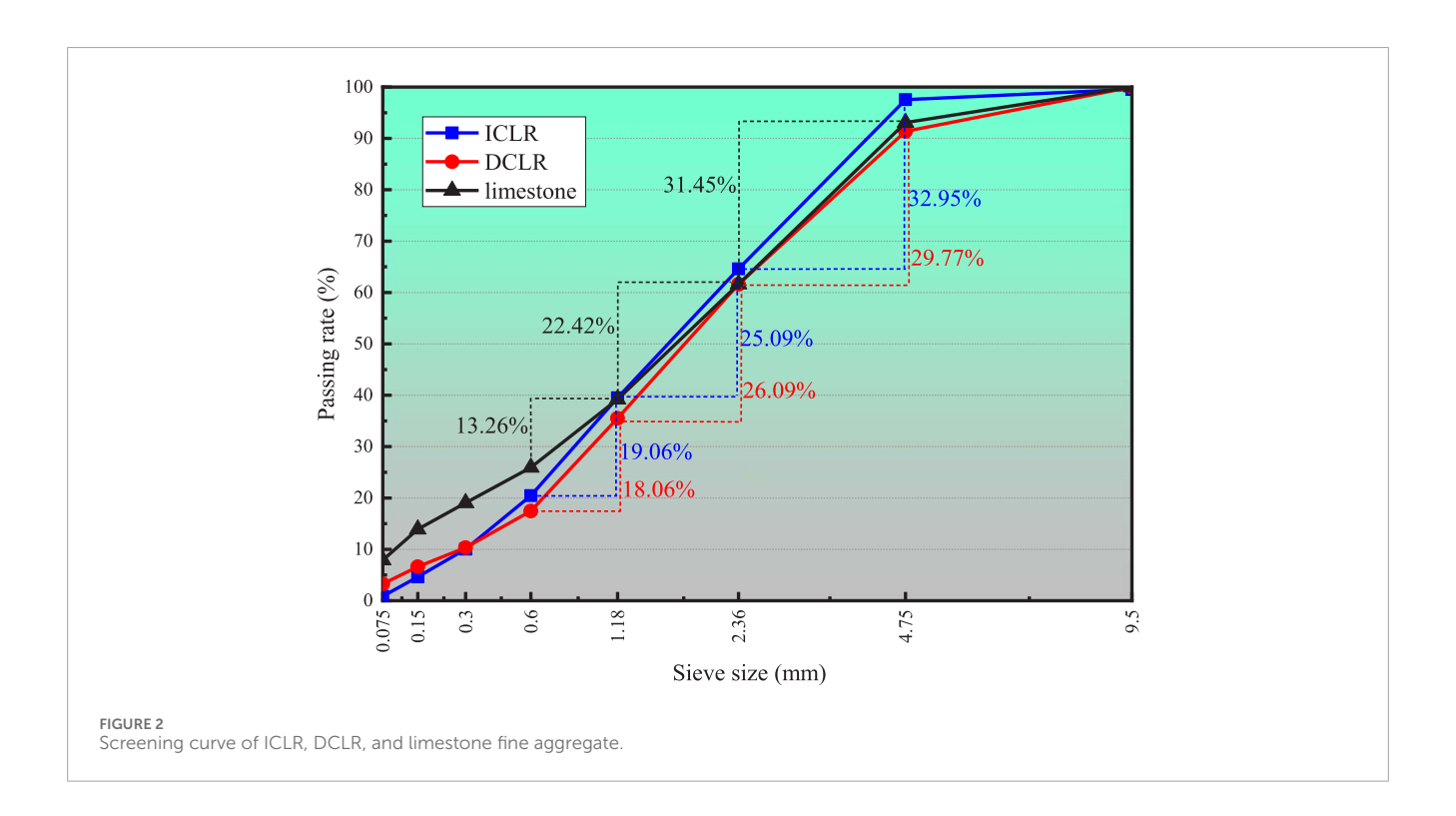
Existing research has primarily focused on DCLR as an asphalt modifier, leveraging its asphaltene content to optimize asphalt's colloidal structure (He, 2013; Fan, 2011). Empirical studies confirm that DCLR enhances asphalt viscosity and temperature resistance, reducing temperature susceptibility by 22%-35% and improving fatigue cracking resistance and deformation recovery by 28%-40% (Ji et al., 2019a; Shi, 2017). Notably, the tetrahydrofuran soluble fraction (THFS) at ≤10% concentration achieves an optimal balance between high-temperature rutting resistance (76% improvement) and medium-temperature fatigue durability (Wu, 2019). However, while additives like ZnO improve UV aging resistance, they compromise DCLR's high-temperature deformation efficacy (Rong et al., 2018a). Functional modeling confirms DCLR's colloidal stabilization mechanism, particularly under thermal stress conditions (Zhang, 2021), with composite modification techniques effectively addressing low-temperature brittleness through compatibilizer integration (Zhai et al., 2019; Liu et al.; Rong et al., 2018b). Field studies reveal DCLR-modified mixtures demonstrate 30%-45% rut depth reduction under 0.7-1.0 MPa loads at 55 °C-70 °C (Zhi et al., 2020), coupled with 18%-25% enhanced limestone adhesion and water stability (Ji et al., 2019; Ji et al., 2018). Rheological models achieve 92% rutting prediction accuracy, while dynamic modulus analyses show DCLR composites exceed SBS-modified asphalt performance by 15%-20% at 15 °C/10Hz, complying with French HMA high-modulus specifications (Ji et al., 2021; Ji et al., 2017). These findings collectively validate DCLR's capacity to improve high-temperature deformation resistance and hydrological stability, though optimal formulation requires careful balancing of modifier ratios and composite material design.

Recent studies demonstrate that indirect coal liquefaction residue (ICLR) effectively enhances asphalt mixture performance when substituting conventional materials. Wang et al. (2022a) revealed ICLR replacement of mineral powder significantly

improves high-temperature asphalt mortar performance while maintaining low-temperature properties (Wang et al., 2022b). Mechanical enhancements include increased indirect tensile strength (Alexander et al., 2018; Rondon-Quintana Hugo et al., 2018) and improved fatigue resistance in dry-processed asphaltstabilized composites (Zhang et al., 2018). Optimal ICLR incorporation (0%-10% content) enhances pavement durability through superior high-temperature stability, water resistance, and snow/ice control capabilities (Ren, 2020; Wang et al., 2015). Particle size optimization studies indicate 0-4.75 mm ICLR elevates 7day compressive strength to 2.2-6.8 MPa, with fly ash additives further improving frost resistance (Hu et al., 2019; Lin et al., 2018). Strategically incorporating 10%–20% of ICLR (0–9.5 mm) optimizes the angle of internal friction and mechanical properties, while maintaining workability (Liu et al., 2015). These collective findings position ICLR as a viable fine aggregate alternative that substantially upgrades asphalt mixture properties across multiple performance metrics. While the existing research predominantly focuses on direct coal liquefaction residue (DCLR) as an asphalt modifier, its potential as a fine aggregate remains underexplored. Although DCLR's natural particle gradation and high asphaltene content suggest rutting resistance benefits, the mechanistic basis for its performance enhancement as aggregate remains unclear. Similarly, studies on indirect coal liquefaction residue (ICLR) applications have been limited to superficial gradation analyses with natural aggregates, lacking systematic investigation into its high-temperature improvement mechanisms or rutting behavior impacts.

Beyond performance considerations, the environmental implications of utilizing industrial byproducts in construction materials are of paramount importance. Extensive leaching tests conducted on both DCLR and ICLR have consistently demonstrated that the leaching concentrations of heavy metals and other potentially harmful elements from these residues fall significantly below the stringent thresholds established by national environmental protection standards (Wang et al., 2022c). This inert behavior is attributed to the encapsulation of any trace elements within the stable carbonaceous matrix of the residue and their subsequent immobilization by the asphalt binder, which acts as an effective sealing agent. Therefore, when incorporated into asphalt mixtures, these residues are rendered environmentally benign, posing no leaching risk to soil or groundwater. This characteristic, combined with their technical benefits, solidifies their potential as sustainable and ecocompatible alternative materials in road engineering, aligning with the principles of industrial symbiosis and circular economy (Ji et al., 2020).





1.1 Research objectives and methodology

The overarching goal of this research is to systematically evaluate and elucidate the mechanisms through which coal liquefaction residue (CLR), specifically Direct Coal Liquefaction Residue (DCLR) and Indirect Coal Liquefaction Residue (ICLR), enhance the rutting resistance of asphalt mixtures when utilized as fine aggregate substitutes. To achieve this, the following specific objectives are defined, alongside the methodologies employed:

Objective 1: To assess the macro-scale rutting performance. The primary objective is to quantitatively evaluate the rutting deformation of asphalt mixtures with volumetrically

replaced fine aggregates (0.6-4.75 mm) by DCLR and ICLR under combined thermal and mechanical loading conditions.

Methodology: Advanced numerical simulations using the Discrete Element Method (DEM) in PFC2D will be conducted. A virtual rutting test model will be developed and calibrated against experimental data. Parametric studies will be performed across a range of temperatures (45 °C, 50 °C, 55 °C, 60 °C) and load pressures (0.7 MPa, 0.8 MPa, 0.9 MPa, 1.0 MPa) to simulate extreme pavement service conditions.

Objective 2: To identify the optimal substitution strategy. A key aim is to determine the most effective single-particle-size fraction of

TABLE 1 Mechanical properties of ICLR, DCLR and limestone fine aggregate.

Experimental project	Test result		
	Fine aggregate of limestone	ICLR	DCLR
Vickers hardness (HV)	246	615	21
Elastic modulus (GPa)	81	98	6.83

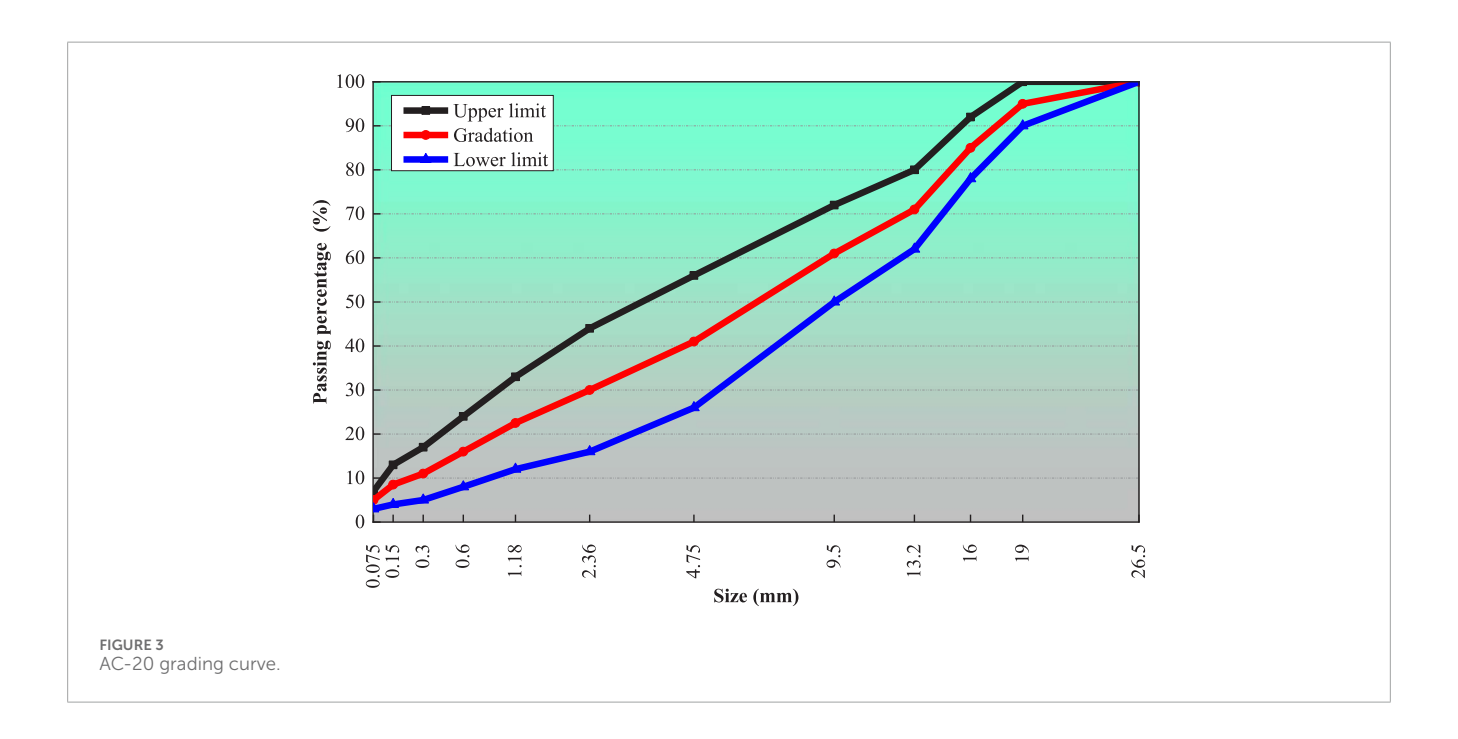


TABLE 2 Alternative scheme for the same particle size and equal volume.

Alternative particle size	Substitution rate
0.6-1.18 mm	6.5%
1.18-2.36 mm	7.5%
2.36–4.75 mm	11%

DCLR and ICLR for replacing conventional limestone fine aggregate to maximize rutting resistance.

Methodology: The rutting performance of mixtures with replacements in three specific size fractions (0.6–1.18 mm, 1.18-2.36 mm, and 2.36-4.75 mm) will be comparatively analyzed against a control mixture. The evaluation will be based on final rut depth, growth rate, and development patterns.

Objective 3: To unravel the underlying micro-mechanical mechanisms. This study seeks to bridge the gap between macro-performance and micro-mechanical behavior by investigating the evolution of force chains and particle displacement within the mixture microstructure during loading.

Methodology: The DEM simulations will be leveraged to analyze the distribution and evolution of contact force chains

and the displacement trajectories of particles of different sizes. This micro-scale analysis will explain the observed macro-scale rutting morphology and performance differences between mixtures containing DCLR, ICLR, and conventional aggregates.

By integrating macro-mechanical performance analysis with micro-mechanical investigation, this research aims to provide a comprehensive understanding of the role of CLR as a functional fine aggregate, offering theoretical and practical guidance for developing high-performance and sustainable asphalt pavements.

The necessity of this research is underscored by three key factors. Resource Utilization: Coal liquefaction residue are abundant byproducts with underutilized potential. Their high-value application in asphalt mixtures aligns with sustainable development goals. Performance Gaps: While DCLR and ICLR show promise, their mechanistic roles as fine aggregates are poorly understood, limiting their practical deployment. Engineering Demand: Rising traffic loads and extreme temperatures necessitate innovative solutions to enhance pavement durability. This study provides a theoretical and practical framework for designing functional aggregates to meet these challenges. By addressing these aspects, our work not only advances the scientific understanding of coal liquefaction residue but also offers actionable insights for their industrial application, paving the way for more sustainable and high-performance asphalt pavements.

TABLE 3 AC-20 grading.

Size (mm)	26.5–19	19–16	16-13.2	13.2-9.5	9.5-4.75	4.75-2.36
Proportion (%)	5	10	14	10	20	11
Size (mm)	2.36-1.18	1.18-0.6	0.6-0.3	0.3-0.15	0.15-0.075	<0.075
Proportion (%)	7.5	6.5	5	2.5	3.5	5

TABLE 4 Adjusted AC-20 grading.

Size (mm)	26.5–19	19–16	16-13.2	13.2-9.5	9.5-4.75	4.75–2.36	2.36-1.18	1.18-0.6
Average diameter (mm)	22.75	17.5	14.6	11.35	7.125	3.555	1.77	0.89
Proportion (%)	6	12	16	12	24	13	9	8

TABLE 5 Number of graded particles.

Size (mm)	19-26.5	16-19	13.2–16	9.5–13.2	4.75-9.5	2.36-4.75	1.18-2.36	0.6-1.18
Number of particles	3	6	12	36	45	242	731	1,447

2 Materials and methods

2.1 Experimental materials

The study employs SK-90 asphalt (Shell Tianjin) combined with limestone aggregates and mineral powder from Beijing sources. DCLR from Shenhua Coal-to-Liquid Chemical Co. (Figure 1a). and ICLR from Lu'an Group (Figure 1b) - both exhibiting black particulate morphology - underwent dust removal, crushing, and screening processes. Comparative particle size analysis with limestone fine aggregates revealed distinct gradation characteristics (Figure 2), with fundamental material properties documented in previous group studies (Wang et al., 2022a; Ji et al., 2020). These coal liquefaction residue, initially solid at ambient temperature, are processed to achieve size compatibility with limestone aggregates and employed in controlled substitution experiments. (Wang et al., 2022b; Ji et al., 2020).

Sieve analysis (Figure 2) reveals comparable particle size distributions among ICLR, DCLR, and limestone fine aggregates, with 0.6–4.75 mm fractions constituting 77.10%, 73.91%, and 67.13%, respectively. While limestone contains elevated sub-0.075 mm particles (12.6% vs. <5% for residues) due to inherent clay content, the remaining fractions show marginal variation. This gradation similarity (Kolmogorov-Smirnov p > 0.05) confirms ICLR/DCLR's potential as limestone substitutes, particularly in the critical 0.6–4.75 mm range governing aggregate interlock.

Vickers hardness and elastic modulus tests were conducted on ICLR, DCLR, and limestone fine aggregates using the MH-500 micro-Vickers hardness tester from China and the Hysitron TI 950 nanoindentation tester from the United States. The results are shown in Table 1.

Table 1 reveals that mechanical characterization reveals significant differences between CLR types and conventional aggregates. ICLR demonstrates superior mechanical performance with 2.5× greater Vickers hardness (615 vs. 246 HV) and 20% higher elastic modulus (98 vs. 81 GPa) compared to limestone aggregates, despite its lower density. This combination of lightweight characteristics and enhanced strength parameters suggests ICLR's potential as a highperformance aggregate alternative. Conversely, DCLR exhibits substantially inferior properties, showing merely 10% of limestone's hardness (21 HV) and modulus (6.8 GPa), indicating inferior deformation resistance. These disparities originate from fundamental structural differences: DCLR's disordered organic molecular arrangement contrasts sharply with limestone's crystalline ionic/metallic bonding, while ICLR's enhanced mechanical properties derive from its optimized particulate structure.

2.2 Experimental methods

Following AC-20 median grading (Figure 3), this study employs volumetric substitution of limestone fine aggregates with size-matched coal liquefaction residue (CLR). The methodology maintains identical particle size distributions and bulk volumes across replacement levels, exemplified by 1.18–2.36 mm CLR particles directly replacing corresponding limestone fractions. This approach preserves aggregate gradation integrity while introducing CLR's unique material properties, with detailed substitution ratios and sieve analyses provided in Table 2.

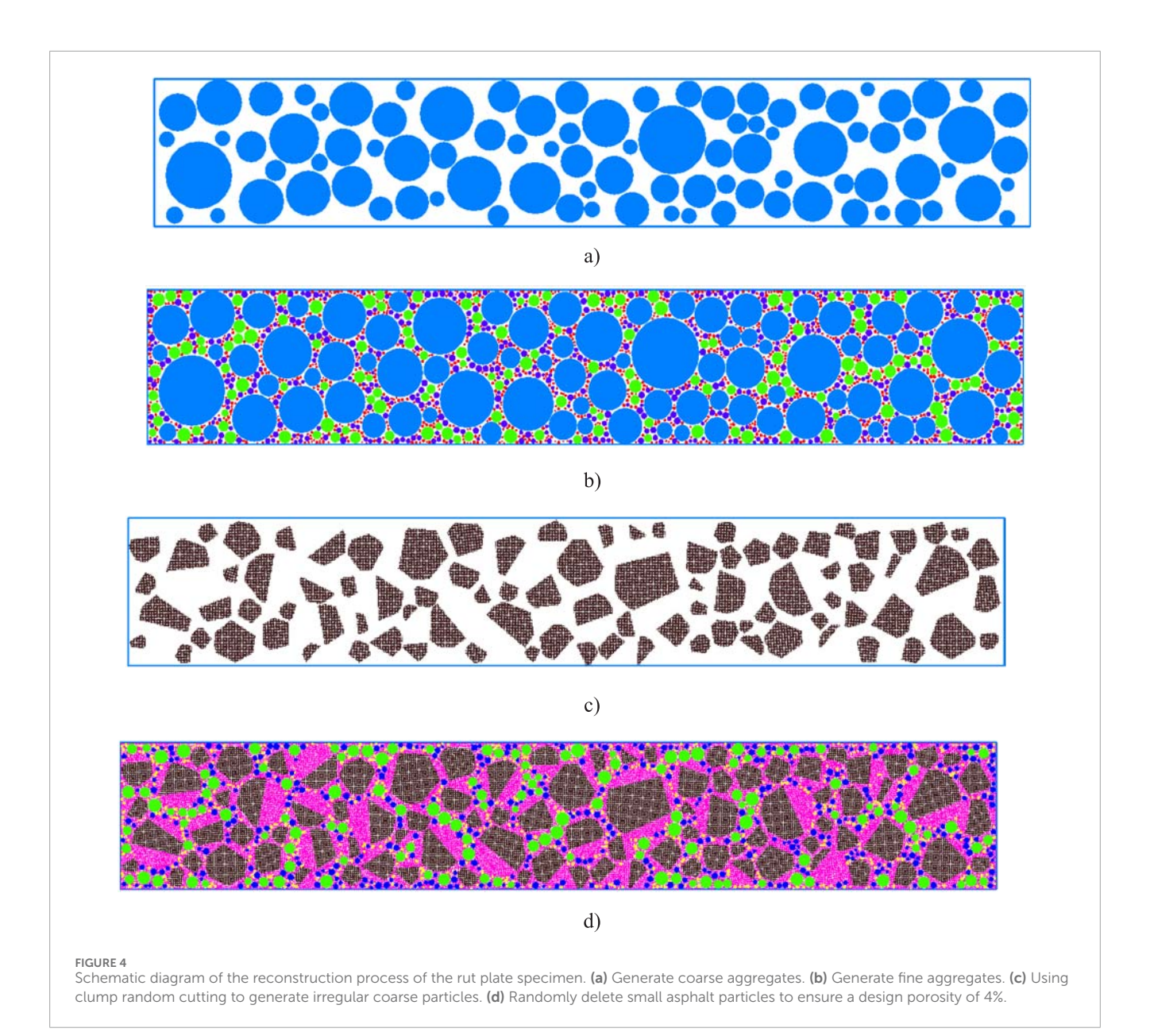


TABLE 6 Bond parameters.

Point bonding parameters	k _n	k _s	cb_tenf	cb_shearf	Fric
Parameter value (N/m)	1×10^8	1×10^8	1×10^4	1×10^4	0.25

3 Numerical modeling and methodology

3.1 Virtual specimen generation

Aggregate morphology in asphalt mixtures exhibits size-dependent characteristics: particles exceeding 4.75 mm display

angular surface geometries, while sub-4.75 mm fractions trend toward sphericity. This study employs distinct geometric representations—spheres for sub-4.75 mm aggregates and polyhedral clusters (5–8 facets formed by finer particle aggregations) for coarser particles. Gradation parameters adhere to standardized specifications, with detailed compositional ratios provided in Table 3.

TABLE 7 Discrete element Burgers model parameters of ICLR asphalt mortar at different temperati	TABLE 7	Discrete element Burge	rs model parameters of ICLR	asphalt mortar at different temperature	S.
---	---------	------------------------	-----------------------------	---	----

Temperature/°C	<i>K_{kn}</i> /10 ⁶ kPa⋅m	$K_{k au}/10^6~\mathrm{kPa\cdot m}$	C _{kn} /10 ⁶ MPa⋅m	C _{kτ} /10 ⁶ MPa·m
45	0.3757	0.1252	0.1280	0.0427
50	0.1838	0.0613	0.0787	0.0262
55	0.1647	0.0549	0.0636	0.0212
60	0.1225	0.0408	0.0451	0.0150
45	1.5974	0.5325	1.5779	0.5260
50	1.2398	0.4133	1.0362	0.3454
55	0.9299	0.3100	0.9033	0.3011
60	0.8123	0.2708	1.1435	0.3812

TABLE 8 Discrete element Burgers model parameters of DCLR asphalt mortar at different temperatures.

Temperature/°C	<i>K_{kn}</i> /10 ⁶ kPa∙m	K _{kτ} /10 ⁶ kPa·m	<i>C_{kn}</i> /10 ⁶ MPa⋅m	C _{kτ} /10 ⁶ MPa·m
45	0.4508	0.1502	0.1536	0.0512
50	0.2205	0.0735	0.0944	0.0314
55	0.1976	0.0658	0.0763	0.0254
60	0.1470	0.0489	0.0541	0.0180
45	1.9168	0.6390	1.8934	0.6312
50	1.4877	0.4959	1.2434	0.4144
55	1.1158	0.3720	1.0839	0.3613
60	0.9747	0.3249	1.3722	0.4574

Particle Flow Code (PFC) simulations face computational inefficiency from excessive sub-0.6 mm particles, which increase entity counts and processing time. To optimize computational economics, sub-0.6 mm fractions were redistributed through mass-proportion adjustments across coarser gradations, employing average diameters per gradation level for particle quantity estimation. The optimized size distribution parameters are detailed in Table 4.

In actual three-dimensional space, each particle has three dimensions, while in PFC2D, it needs to be converted into an area index to calculate the specific number of particles generated for each aggregate level. Currently, there are two particles, and according to mathematical relationships:

Particle 1:
$$V_1 = \frac{4}{3}\pi r_1^3$$

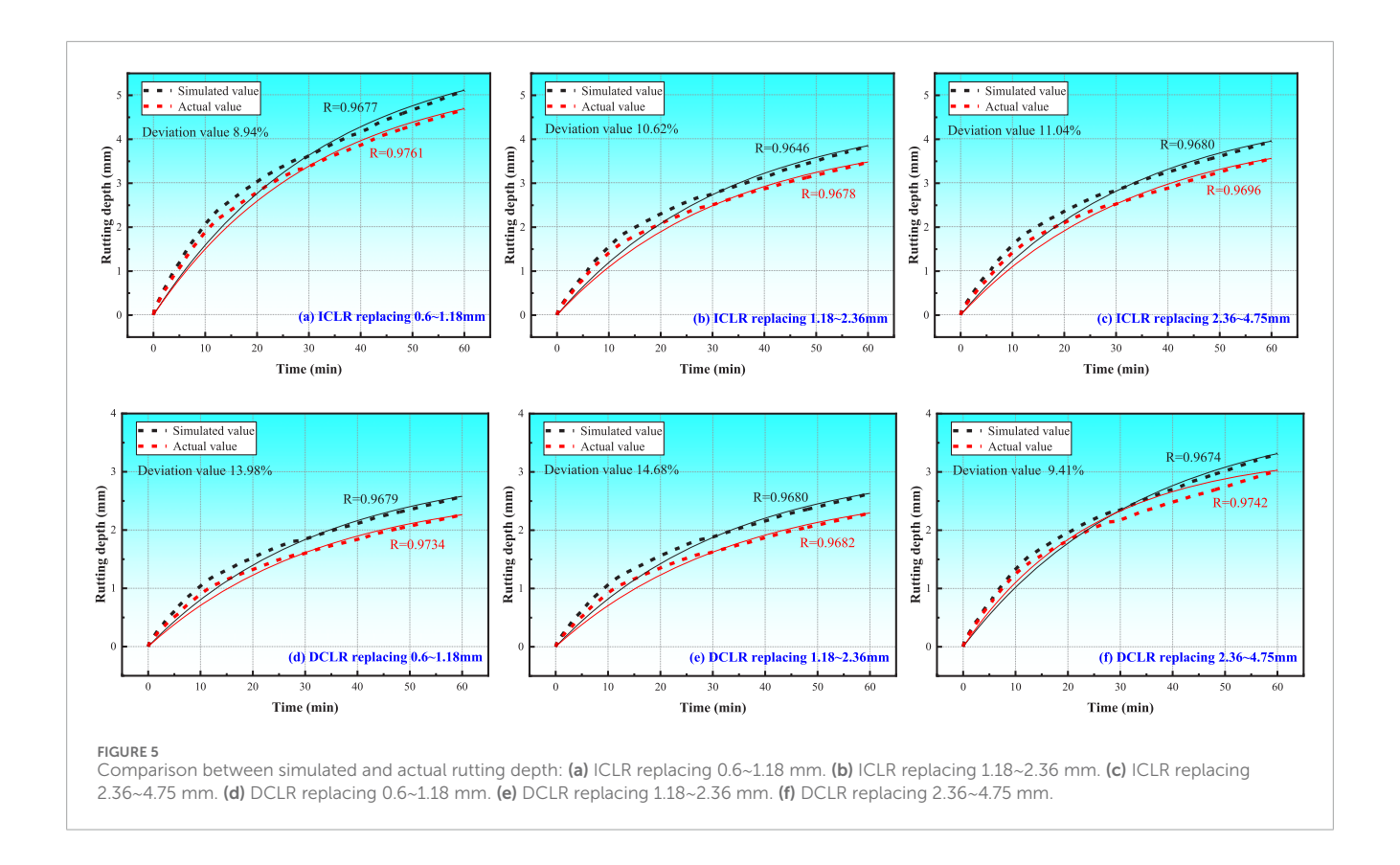
Particle 2: $V_2 = \frac{4}{3}\pi r_2^3$

The volume ratio of the two particles is: $\frac{V_1}{V_2} = \frac{\frac{4}{3}\pi r_1^3}{\frac{4}{3}\pi r_2^3} = \frac{r_1^2 \cdot r_1}{r_2^2 \cdot r_2} = \frac{S_1 \cdot r_1}{S_2 \cdot r_2}$ The volume ratio (V_1/V_2) of two particles is equal to the area ratio (S_1/S_2) , multiplied by a coefficient, which is the radius ratio (r_1/r_2) of the two small balls. By converting the volume ratio of particles in three-dimensional

space into the area ratio, the following relationship can be obtained:

$$\begin{split} \frac{V_1}{V_2} &= \frac{S_1}{S_2} \times \frac{r_1}{r_2} = \frac{S_1}{S_2} \times \frac{11.375}{8.75} = \frac{6\%}{12\%} & S_1 = \frac{6\%}{12\%} \times \frac{8.75}{11.375} \times S_2 \\ \frac{V_2}{V_3} &= \frac{S_2}{S_3} \times \frac{r_2}{r_3} = \frac{S_2}{S_3} \times \frac{8.75}{7.3} = \frac{12\%}{16\%} & S_2 = \frac{12\%}{16\%} \times \frac{7.3}{8.75} \times S_3 \\ \frac{V_3}{V_4} &= \frac{S_3}{S_4} \times \frac{r_3}{r_4} = \frac{S_3}{S_4} \times \frac{7.3}{5.675} = \frac{16\%}{12\%} & S_3 = \frac{16\%}{12\%} \times \frac{5.675}{7.3} \times S_4 \\ \frac{V_4}{V_5} &= \frac{S_4}{S_5} \times \frac{r_4}{r_5} = \frac{S_4}{S_5} \times \frac{5.675}{3.5625} = \frac{12\%}{24\%} & S_4 = \frac{12\%}{24\%} \times \frac{3.5625}{5.675} \times S_5 \\ \frac{V_5}{V_6} &= \frac{S_5}{S_6} \times \frac{r_5}{r_6} = \frac{S_5}{S_6} \times \frac{3.5625}{1.7775} = \frac{24\%}{13\%} & S_5 = \frac{24\%}{13\%} \times \frac{1.7775}{3.5625} \times S_6 \\ \frac{V_6}{V_7} &= \frac{S_6}{S_7} \times \frac{r_6}{r_7} = \frac{S_6}{S_7} \times \frac{1.7775}{0.885} = \frac{13\%}{9\%} & S_6 = \frac{13\%}{9\%} \times \frac{0.885}{0.885} \times S_8 \\ \frac{V_7}{V_8} &= \frac{S_7}{S_8} \times \frac{r_7}{r_8} = \frac{S_7}{S_8} \times \frac{0.885}{0.445} = \frac{9\%}{8\%} & S_7 = \frac{9\%}{8\%} \times \frac{0.445}{0.885} \times S_8 \end{split}$$

Aggregate particle quantification in PFC2D employs areabased scaling, where the total aggregate area divided by the



individual particle area determines particle counts. To reconcile model fidelity with computational efficiency, AC-20 gradations undergo dimensional adaptation: 3D volumes are converted to 2D area ratios (1-unit thickness assumption) without radius scaling. Calibration revealed optimal 0.6–1.18 mm particle counts at \sim 1,447 to achieve realistic rutting section representation, requiring systematic reduction of fine particles to match empirical observations. Final modeled particle distributions across gradations are quantified in Table 5, demonstrating effective balance between geometric accuracy and simulation feasibility.

The model generated in PFC is shown in Figure 4.

3.2 Loading principle

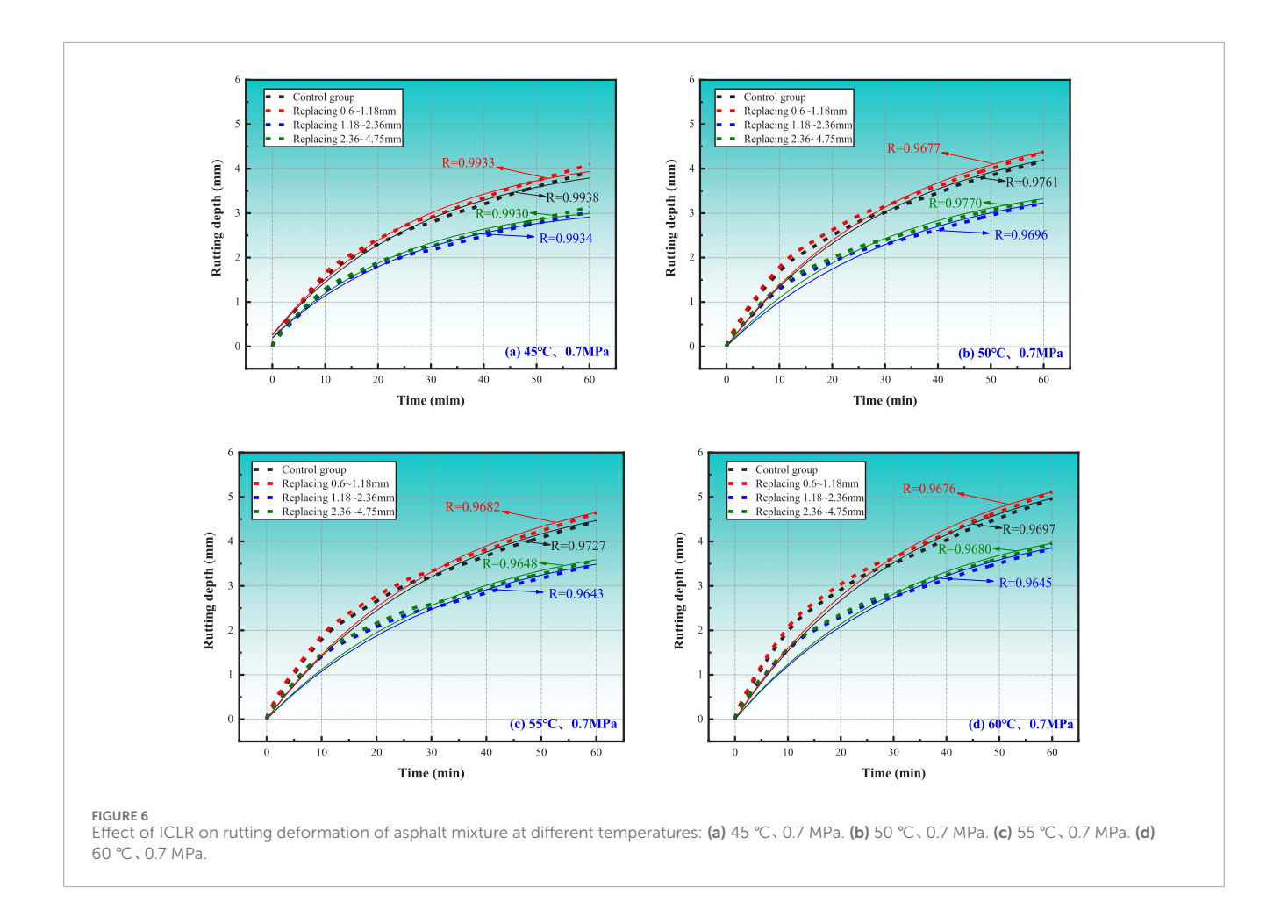
According to the "Test Specification for Asphalt and Asphalt Mixtures in Highway Engineering" (JTG E20-2011) (Ministry of Transport of the People's Republic, 2011), the outer diameter of the rubber tire is 200mm, the wheel width is 50mm, the mass of the rubber wheel is 78kg, the load pressure is 0.7MPa, the distance the rubber wheel rolls along the middle of the rutting plate is 230mm, the wheel rolling speed is 42 cycles per minute, and the test temperature is set at 60 °C. Given the differences between the model loading method in PFC and the actual rutting test, an equivalent static load method can be employed. The cumulative time of the wheel load reciprocating action at a specific point during the

actual rutting test can be equated to the static loading time in the two-dimensional virtual rutting test. The correlation is as follows:

$$m \cdot g = p \cdot d \cdot l$$

In the formula, m represents the mass of the rubber wheel; G is the gravitational acceleration; P is the load pressure; D is the width of the rubber wheel; L is the contact length between the rubber wheel and the surface of the rut specimen, which is 21.84 mm according to indoor tests. Therefore, it can be simplified to using a wall loading method, using a servo program to maintain a contact pressure of 0.7 MPa, with an action time of $3600 \times l/230 = 342s$, and adjusting the wall speed to ensure that the contact force reaches the target pressure. When simulating temperature, it is necessary to change the Burgers model parameters corresponding to different temperatures in the PFC code to achieve the simulation of rutting deformation under different temperatures and loads.

Given China's summer asphalt pavement temperatures (45 °C–60 °C) and increasing traffic overloading (tire pressures \geq 0.7 MPa, frequently exceeding 1.0 MPa), this study simulates rutting deformation through controlled parametric testing. Rutting simulations were conducted across four temperature levels (45 °C, 50 °C, 55 °C, 60 °C) and four load pressures (0.7–1.0 MPa, 0.1 MPa increments). This 4 × 4 factorial design specifically examines: (1) thermal effects on rutting at 60 °C under varying loads, and (2) mechanical responses under 0.7 MPa pressure across temperature gradients, replicating extreme operational conditions of modern highway pavements.



3.3 Model and parameters

3.3.1 Aggregates

The discrete element framework employs rigid clusters (geometrically invariant) and compressible flexible clusters to simulate asphalt mixtures, with aggregate particles represented as size-graded spheres. Coarse aggregates (>4.75 mm) are modeled using Clump random tessellation algorithms to replicate angular morphologies, while sub-4.75 mm particles retain spherical geometries. This dual-morphology approach preserves aggregate structural integrity while enabling mechanical response differentiation between particle size fractions.

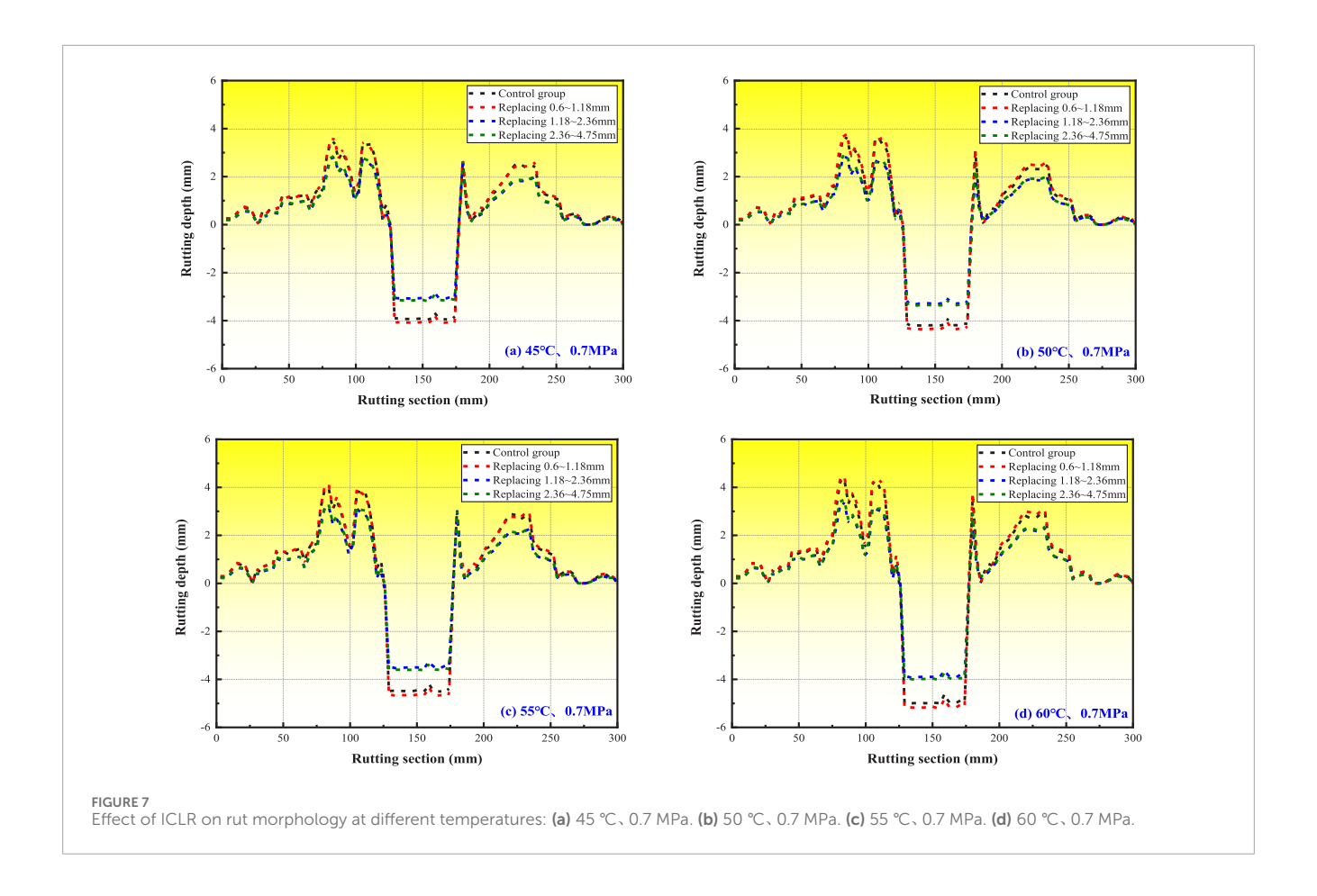
In general, the normal stiffness Kn and tangential stiffness Ks of limestone aggregate are set to $1\times 108 \text{N/m}$, and the density of the aggregate is set to $2600~\text{kg/m}^3$. Since the density of ICLR in this study is slightly smaller than that of limestone fine aggregate, but the hardness and modulus are larger than those of limestone fine aggregate, based on the density and hardness relationship between ICLR and limestone fine aggregate, the parameter settings of the discrete element after replacing fine aggregate with ICLR in this study are: the density is set to $2500~\text{kg/m}^3$, and the normal stiffness Kn and tangential stiffness Ks are both set to $1.2\times 108 \text{N/m}$; The DCLR density is set to $1208~\text{kg/m}^3$, and the normal stiffness Kn and tangential stiffness Ks are both set to $1.2\times 107 \text{N/m}$.

The bonding model between aggregates selects point bonding, where there will be no sliding between the two particles, and the effect will only be on the contact point, transmitting only force and not torque. The calibration is mainly carried out through four parameters: normal and tangential stiffness, tensile strength, and shear strength, namely, kn, ks, cb_tenf, and cb_shearf. The friction coefficient is usually set at 0.25, and the parameter settings are shown in Table 6.

3.3.2 Asphalt mortar

The viscoelastic behavior of asphalt mixtures under elevated temperatures (45 °C–60 °C) was simulated using the Burgers model, with parameters calibrated from prior studies (Fan, 2014; Peng, 2016; Gao, 2018). While DCLR incorporation as fine aggregate introduces 3% asphaltenes and 1.5% maltenes (saturates/aromatics/resins) that enhance asphalt adhesion through interfacial interactions, current models cannot fully capture DCLR's particulate morphology effects.

Experimental evidence demonstrates that a 10% DCLR content (1:10 mass ratio) triples asphalt's adhesion strength (Ji et al., 2015; Chen, 2019). Therefore, when DCLR replaces fine aggregates of a single particle size, specifically 0.6 mm (6.5%), 1.18 mm (7.5%), or 2.36 mm (11%), with an average DCLR substitution rate of 8.33%, the ratio of melted DCLR to matrix asphalt is approximately 1:25. To



obtain the microscopic parameters of the asphalt mortar after DCLR replaces fine aggregates, the parameters of the discrete - element Burgers model for ordinary asphalt mortar should be multiplied by 3 (10/25), which is 1.2 times. The relevant parameters are shown in Tables 7 and 8.

Model validity was verified through comparative analysis of simulated and experimental rutting behaviors under 60 °C/0.7 MPa conditions. ICLR/DCLR-substituted asphalt mixtures exhibited strong congruence between experimental and simulated rutting progression (Figure 5), with maximum depth discrepancies limited to 11.04% (ICLR) and 14.68% (DCLR). These error margins confirm the model's capacity to capture critical deformation mechanisms while maintaining computational fidelity. The sub-15% deviations across substitution types validate the parameter selection framework, establishing a robust numerical foundation for asphalt mixture rutting analysis under varied material compositions.

4 Results and analysis

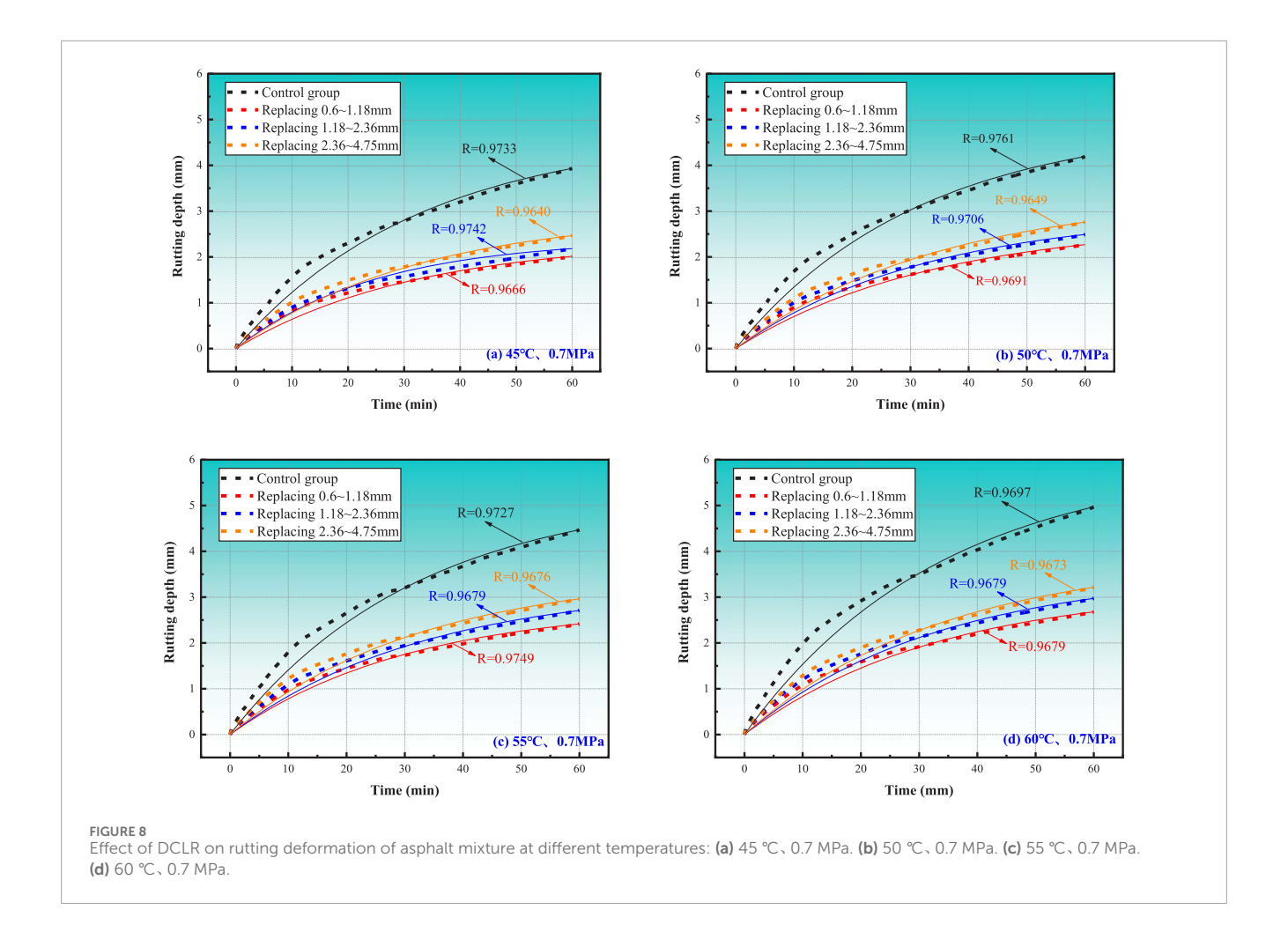
4.1 The influence of temperature on the rutting behavior of asphalt mixture

4.1.1 The influence of ICLR on rutting behavior 4.1.1.1 Rutting depth

Figure 6 shows the development law of rutting deformation of asphalt mixture after replacing fine aggregate with ICLR under the

standard load of 0.7 MPa and four different temperatures of 45 °C, 50 °C, 55 °C, and 60 °C.

- 1. As shown in Figure 6, All four asphalt mixtures exhibited consistent rutting development trends across the four test temperatures, with rut depth demonstrating exponential growth. (correlation coefficients >0.9). When fine aggregates are replaced with ICLR, the rut growth rate analysis reveals three distinct stages: 0–10 min (maximum growth rate), 10–20 min (decelerating rate), and 20–60 min (stabilized linear trend). The first 20 min constitute the critical period for rut formation, as the mixture's higher void ratio and greater plasticity during this phase make it more susceptible to compaction. Subsequently, reduced voids and increased density enhance resistance to deformation, resulting in diminished rutting progression.
- 2. Both control and experimental groups showed increasing rut depth with rising temperature. Replacing 0.6–1.18 mm aggregates consistently increased rut depth compared to controls, while substitutions of 1.18–2.36 mm and 2.36–4.75 mm aggregates reduced rut depth. At 45 °C–60 °C, rut depth changes relative to controls were: +2.93–4.54% (0.6–1.18 mm), -21.97%–22.94% (1.18–2.36 mm), and -19.69%–24.66% (2.36–4.75 mm). The 1.18–2.36 mm replacement demonstrated the optimal rutting resistance, followed by the 2.36–4.75 mm fraction, while the 0.6–1.18 mm performed worst. This poor performance stems from: 1)



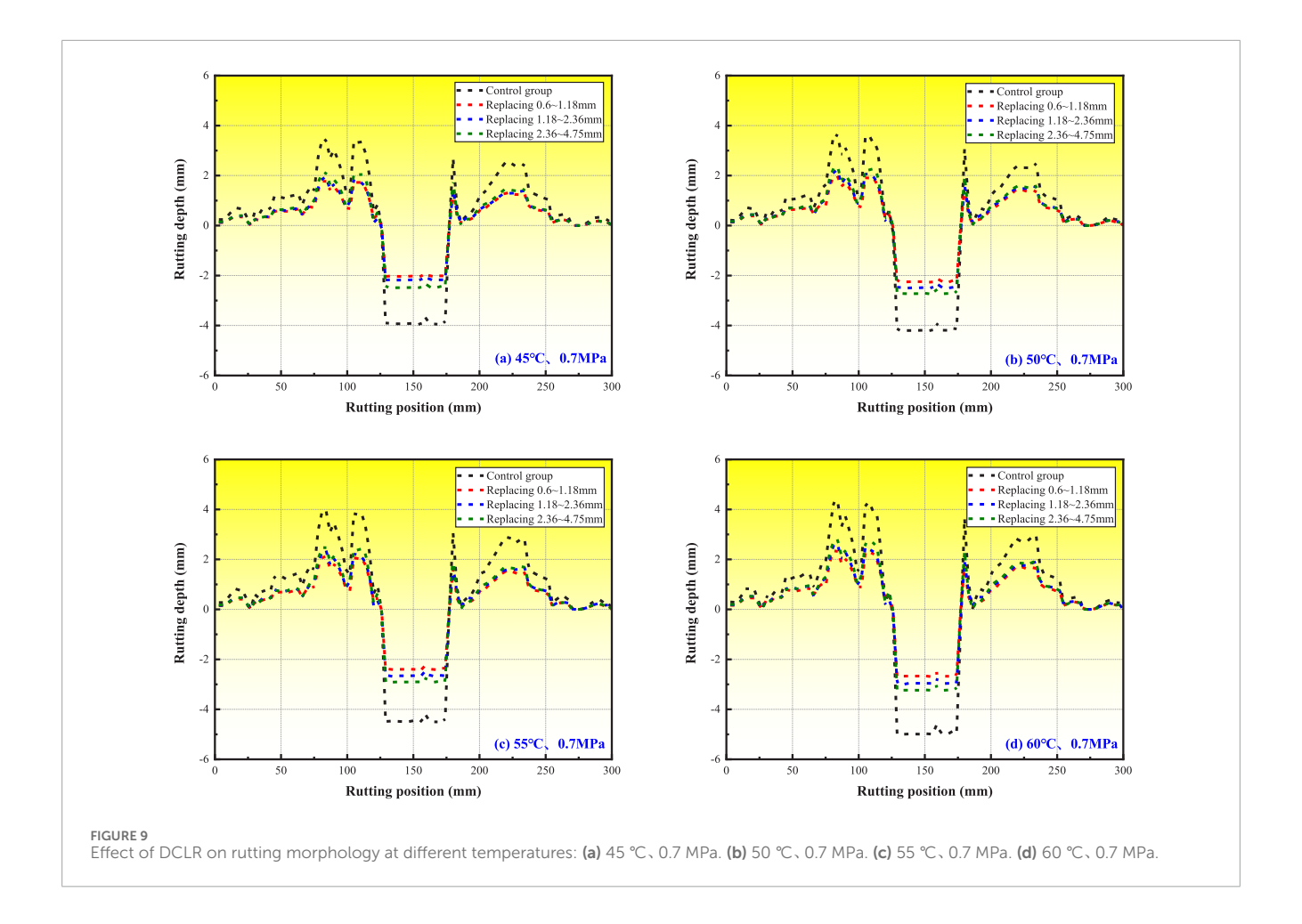
insufficient substitution quantity to leverage ICLR's high modulus/hardness due to finer particle size, and 2) smaller pore volume and weaker asphalt adhesion in 0.6–1.18 mm ICLR compared to limestone aggregates, compromising high-temperature performance.

4.1.1.2 Rutting deformation

The rut morphology refers to the displacement distribution of particles perpendicular to the wheel travel direction after rolling. Figure 7 illustrates the rutting deformation *versus* longitudinal position for asphalt mixtures with ICLR-replaced fine aggregates under 0.7 MPa load at 45 °C–60 °C. The horizontal axis represents the model's longitudinal direction (perpendicular to wheel movement), corresponding to the rut plate's length in our 2D model.

1. Figure 7 reveals that rutting protrusions perpendicular to wheel travel occur primarily within 75–125mm and 175–225 mm ranges at 45 °C–60 °C, while being minimal at 0–50mm and 250–300 mm. While theoretically symmetrical in uniformly distributed aggregate models, the discrete element method's random particle distribution causes asymmetry. Notably, finer particle models exhibit reduced symmetry differences, resulting in smaller variations between bilateral rutting protrusions.

- 2. Under constant load, rutting protrusions in the 75–125 mm and 175–225 mm longitudinal ranges reach heights of 1–4.2mm and 0–4mm, respectively, across four temperatures (45 °C–60 °C). This behavior stems from particle size distribution differences the left side's higher concentration of fine particles exhibits reduced resistance to lateral wheel pressure compared to coarse particles. Temperature increases induce distinct deformation patterns: the left wheel side shows spiral-increasing rutting with dual peaks (75–125 mm), while the right side displays spiral-decreasing deformation featuring both sharp and wide peaks (175–225 mm), revealing coarse particles at valleys flanked by fine particles.
- 3. Peak growth rates from 45 °C to 60 °C were 29.3% (control), 27.10% (0.6–1.18 mm), 19.46% (1.18–2.36 mm), and 15.02% (2.36–4.75 mm). The raised peak beneath the wheel indicates combined longitudinal and lateral particle displacement, with coarse particles underlying this feature. Rut depth correlates with load magnitude, while protrusion height varies by mixture type: 0.6–1.18 mm replacements match control group behavior, whereas 1.18–2.36 mm and 2.36–4.75 mm substitutions demonstrate comparable rutting curves with minimal depth variations.



4.1.2 The influence of DCLR on rutting behavior 4.1.2.1 Rutting depth

Figure 8 shows the development of rutting deformation in asphalt mixtures after replacing fine aggregates with DCLR under the standard load of 0.7 MPa and four different temperatures of 45 °C, 50 °C, 55 °C, and 60 °C.

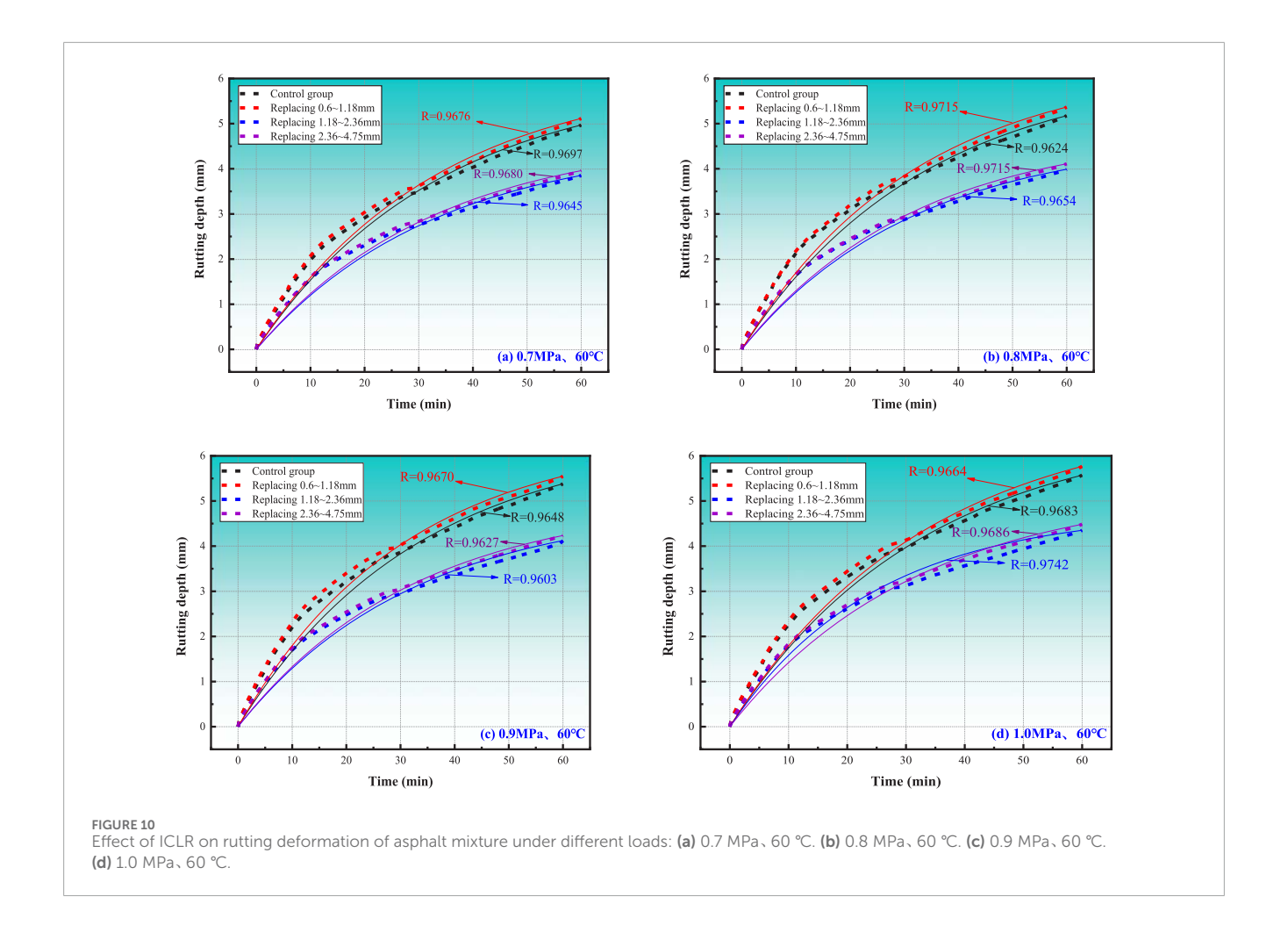
- 1. Figure 8 reveals that all four asphalt mixtures exhibit similar rutting development trends when fine aggregates are replaced with either ICLR or DCLR, showing a power-function increase in rut depth over time (correlation coefficients >0.9). For DCLR-modified mixtures, the rutting growth progresses through three distinct phases: rapid initial growth (0–10 min), transitional deceleration (10–20 min), and stable development (20–60 min). Notably, both ICLR and DCLR replacements demonstrate comparable rutting patterns, with the first 20 min representing the critical period for deformation when the mixtures exhibit their poorest high-temperature resistance.
- 2. Both control and experimental groups exhibited progressively increasing rut depth with rising temperature (45–60 °C). When DCLR replaced fine aggregates, rut depth followed this order: control >2.36–4.75 mm > 1.18–2.36 mm > 0.6–1.18 mm mixtures. Relative to controls, rut depth reductions at all temperatures were most substantial for 0.6–1.18 mm replacements (–45.88%

to -48.81%), followed by 1.18-2.36 mm (-39.37% to -44.49%) and 2.36-4.75 mm (-33.73% to -37.31%). These results demonstrate DCLR's effectiveness in enhancing rut resistance, with 0.6-1.18 mm substitutions providing optimal high-temperature performance improvement.

4.1.2.2 Rutting deformation

Figure 9 shows the relationship between the longitudinal position of the asphalt mixture model and rutting deformation after replacing fine aggregates with DCLR under standard load of 0.7 MPa and four temperatures of 45 °C, 50 °C, 55 °C and 60 °C.

- 1. Figure 9 demonstrates that DCLR replacement produces rutting morphology development patterns similar to ICLR, with primary protrusions occurring within 75–125mm and 175–225 mm ranges across the 45 °C–60 °C temperature spectrum, while remaining minimal in the 0–50 mm and 250–300 mm peripheral zones.
- Under constant load conditions, the experimental group exhibited rut protrusion heights of 0.5–2.5 mm (75–125 mm range) and 0–3 mm (175–225 mm range). Among the four mixtures, the control group showed the highest rutting, followed by 2.36–4.75mm, 1.18–2.36mm, and 0.6–1.18 mm



replacements. From 45 °C to 60 °C, peak growth rates reached 27.07% (control), 31.41% (0.6–1.18 mm), 35.67% (1.18–2.36 mm), and 30.28% (2.36–4.75 mm).

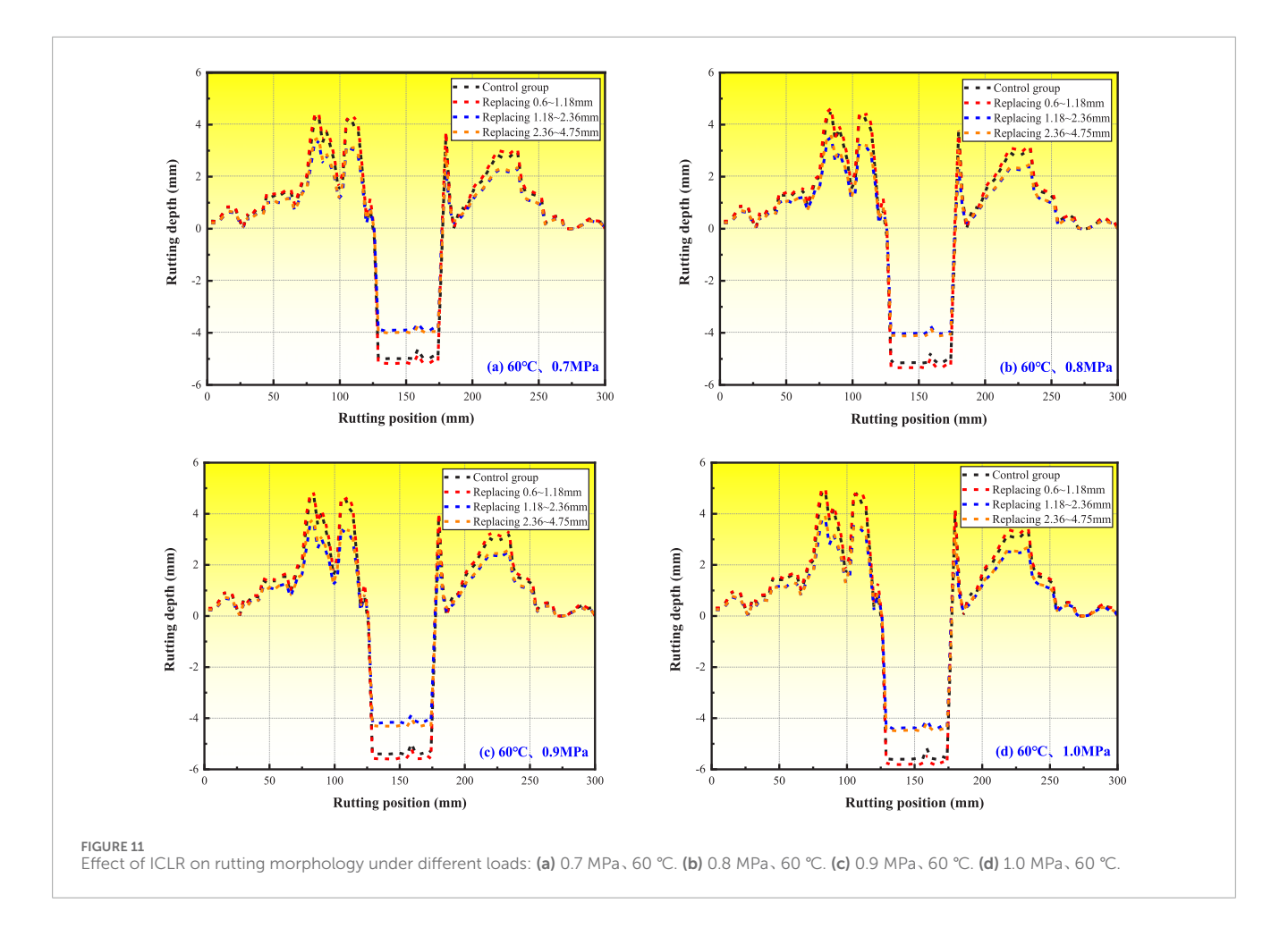
4.2 The influence of load on the rutting behavior of asphalt mixture

4.2.1 The influence of ICLR on rutting behavior 4.2.1.1 Rutting depth

Figure 10 shows the development pattern of rutting deformation of asphalt mixture after replacing fine aggregate with ICLR under the standard temperature of $60\,^{\circ}\text{C}$ and four different loads of 0.7MPa, 0.8MPa, 0.9MPa, and 1.0 MPa.

Figure 10 demonstrates consistent rutting development trends across four loading conditions, mirroring temperature-dependent behavior. Under standard load (0.7 MPa), temperature increases from 45 °C to 60 °C caused rut depth increments of 26.38% (control), 24.78% (0.6–1.18 mm), 27.15% (1.18–2.36 mm), and 33.62% (2.36–4.75 mm). Conversely, at 60 °C, load increases from 0.7MPa to 1.0 MPa resulted in smaller growth rates: 12.12%–13.27%. These results indicate that temperature exerts a greater

- influence on rutting deformation than mechanical loading.
- 2. Under all loading conditions, rut development follows a consistent three-phase pattern: initial exponential growth (0–10 min) with maximum deformation rates, transitional deceleration (10–20 min), and stabilized linear progression (20–60 min). The critical deformation period occurs within the first 20 min, accounting for the most significant rut formation, while the subsequent 40 min exhibit gradual, linear development.
- 3. ICLR-modified asphalt mixtures exhibit distinct rutting performance across two gradients: (1) 2.36–4.75mm and 1.18–2.36 mm replacements showing superior performance, and (2) 0.6–1.18 mm replacements performing similarly to the control group. Across all temperatures and loading conditions (0.7–1.0 MPa), rut depth consistently followed this order: 0.6–1.18 mm > control >2.36–4.75 mm > 1.18–2.36 mm. Quantitative analysis revealed rut depth changes relative to controls: +2.93–3.69% (0.6–1.18 mm), -21.92%–23.36% (1.18–2.36 mm), and -19.52%–21.28% (2.36–4.75 mm). These results demonstrate that 1.18–2.36 mm replacement provides optimal rut resistance, followed by 2.36–4.75mm, while 0.6–1.18 mm substitution shows minimal improvement over conventional mixtures.



4.2.1.2 Rutting deformation

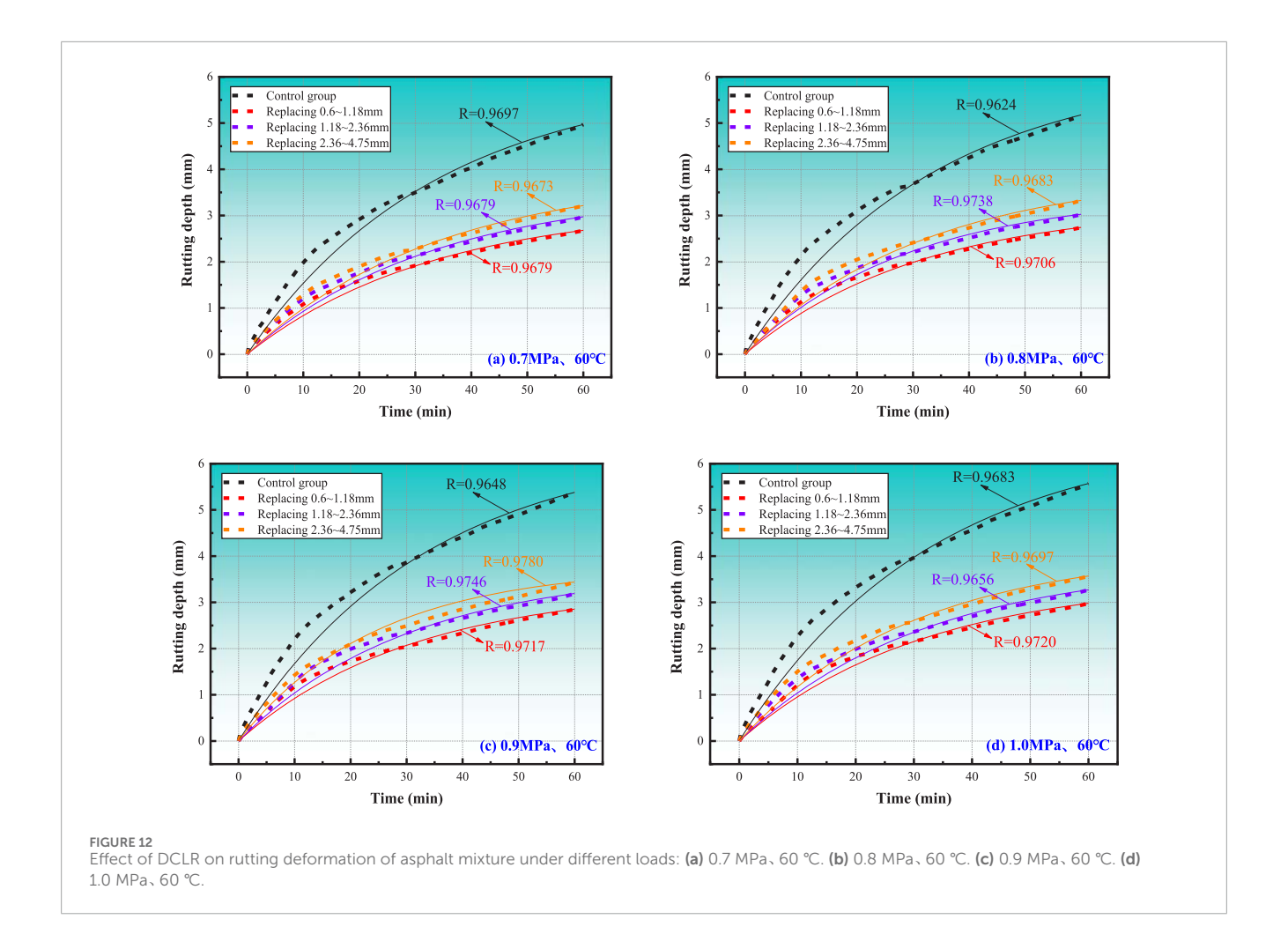
Figure 11 shows the relationship between the longitudinal position of the asphalt mixture model and rutting deformation after replacing fine aggregates with ICLR under standard temperature of 60 °C and four different loads of 0.7MPa, 0.8MPa, 0.9MPa and 1.0 MPa.

- 1. From Figure 11, it can be seen that when the load changes from 0.7 MPa to 1.0 MPa, the position where the rut bulge still occurs in the direction of vertical wheel travel is within the range of 75–125mm and 175–225 mm. The rut bulge is relatively small in the range of 0–50mm and 250–300 mm on both sides.
- 2. Under constant temperature conditions, the test group exhibited rut protrusion heights of 1-5 mm (75-125 mm range) and 0-4 mm (175-225 mm range) across four loading conditions (0.7-1.0 MPa). Increasing load induced spiral deformation patterns in wheel paths, maintaining characteristic peak profiles (twin peaks at 75-125mm; sharp/broad peaks at 175-225 mm). Peak growth rates ranged 11.45%-13.26%, confirming temperature's greater influence than load on rut formation. Rut height progression followed similar trends: 0.6–1.18 mm replacements matched control group behavior, while 1.18-2.36 mm and 2.36-4.75 mm substitutions demonstrated comparable performance.

4.2.2 The influence of DCLR on rutting behavior 4.2.2.1 Rutting depth

Figure 12 shows the development pattern of rutting deformation of asphalt mixture after replacing fine aggregate with DCLR under the standard temperature of 60 $^{\circ}$ C and four different loads of 0.7MPa, 0.8MPa, 0.9MPa, and 1.0 MPa.

- 1. Figure 12 reveals that DCLR-modified mixtures exhibit rutting trends similar to ICLR under various loads. At standard load (0.7 MPa), temperature increases (45 °C–60 °C) caused rut depth growth of 26.38% (control), 33.10% (0.6–1.18 mm), 36.20% (1.18–2.36 mm), and 30.42% (2.36–4.75 mm). In contrast, load increases (0.7–1.0 MPa) at 60 °C produced smaller increments (10.03%–12.12%). These results demonstrate that: (1) temperature effects outweigh load impacts on rut deformation, and (2) DCLR outperforms ICLR in rut resistance, showing reduced sensitivity to thermal/mechanical variations and superior high-temperature performance.
- 2. All four mixtures demonstrate consistent rutting development across loading conditions, mirroring the ICLR replacement pattern. The deformation progresses through three distinct phases: rapid power-function growth (0–10 min), transitional deceleration (10–20 min), and stabilized linear growth (20–60 min). The critical deformation period occurs within the first 20 min, accounting for the most significant rut



formation, while subsequent development shows gradual, linear progression. This three-stage evolution confirms 0–20 min as the crucial timeframe for rut development under various loading conditions.

3. Both control and experimental groups exhibited increasing rut depth with higher loads. DCLR replacement produced two distinct performance tiers: (1) control group showing highest rutting, and (2) modified mixtures with 0.6–1.18 mm > 1.18–2.36 mm > 2.36–4.75 mm replacements demonstrating superior resistance. At loads of 0.7–1.0MPa, rut depth reductions relative to controls were most significant for 0.6–1.18 mm replacements (–46.08% to –47.01%), followed by 1.18–2.36 mm (–40.17% to –41.53%) and 2.36–4.75 mm (–35.30% to –36.06%). These results establish that 0.6–1.18 mm DCLR substitution provides optimal rut resistance in single-size replacements.

4.2.2.2 Rutting deformation

Figure 13 shows the relationship between the longitudinal position of the asphalt mixture model and rutting deformation after replacing fine aggregates with DCLR under four different loads of 0.7MPa, 0.8MPa, 0.9MPa and 1.0 MPa at a standard temperature of 60 °C.

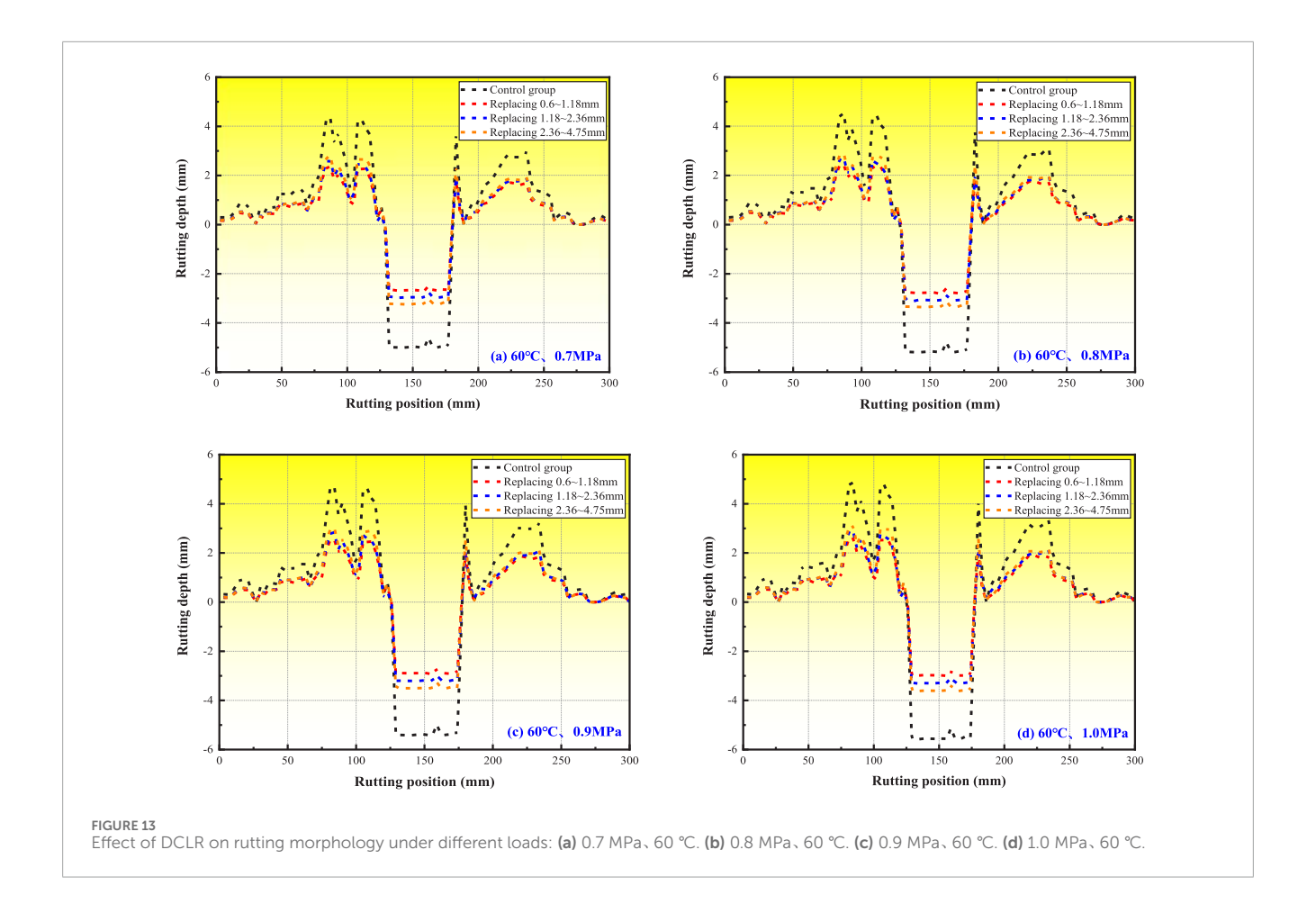
1. From Figure 13, it can be seen that after replacing fine aggregate with DCLR, the load changed from 0.7 MPa to

- 1.0 MPa, and the location of rut protrusion remained within the range of 75–125mm and 175–225mm, with smaller rut protrusions within the range of 0–50mm and 250–300 mm on both sides.
- 2. Under constant temperature conditions, the four asphalt mixtures exhibited rut protrusion heights of 1–2.8 mm (75–125 mm range) and 0–2 mm (175–225 mm range). Increasing load from 0.7 to 1.0 MPa produced growth rates of 11.51%–13.46%, confirming temperature's greater influence than load on rut formation. Rut depth followed this hierarchy: control group >2.36–4.75 mm > 1.18–2.36 mm > 0.6–1.18 mm replacements, with the finest aggregate substitution showing optimal resistance.

4.3 The influence of microstructure on rutting behavior

4.3.1 The influence of force chain distribution on rutting

The macroscopic rutting behavior of asphalt mixtures correlates with their microscopic structure, characterized by force chain distribution and particle displacement patterns. This study examines the DCLR-modified mixture (2.36 mm replacement) and SK-90 control group under standard conditions (60 °C,



0.7 MPa), analyzing force chain transmission during three rutting phases: rapid formation (0–10 min), transition (10–20 min), and stabilization (20–60 min). The slope of the rut curve changes rapidly between 0 and 10 min, increases more gradually between 10 and 20 min, and increases most slowly between 20 and 60 min. Therefore, the model study divides the rut changes into three stages. The investigation focuses on the interrelationship between particle displacement and force chain evolution to elucidate microstructural mechanisms governing rut development.

The two-dimensional model is equivalent to a three-dimensional contact network through the force chain density per unit length in the thickness direction. By adjusting the boundary conditions of the two-dimensional model, the contact force chains and lateral displacement of three-dimensional particles can be approximated. Studies (Fan, 2014; Gao, 2018) have shown that the prediction error of the two-dimensional model for rutting deformation is less than 10%, and the anisotropy error caused by the two-dimensional simplification can be neglected.

4.3.1.1 Initial loading stage

Figure 14 shows the force schematic diagram of DCLR single particle size replacement of 2.36–4.75 mm fine aggregate and SK-90 asphalt mixture at the initial 10 min of loading.

- 1. Figure 14 demonstrates that particle deformation under load produces distinct force chain patterns: quasi-linear strong chains (high force transmission, dense distribution) versus sparse weak chains (low force transmission) (Peng, 2016; Mingfeng et al., 2018). The DCLR-modified mixture (2.36–4.75 mm replacement) exhibits sparser force chains in the wheel path compared to the denser control group distribution. This difference arises because DCLR enhances high-temperature resistance, reducing particle displacement and collision forces, while the conventional mixture's greater particle movement generates more intensive force chain networks under identical loading conditions.
- 2. In uncompacted regions beyond the wheel path, the DCLR-modified mixture (2.36–4.75 mm replacement) exhibits denser force chains compared to the control group's sparse distribution. This contrast stems from DCLR's composite modification effect, DCLR particles dissolve in asphalt. On the one hand, the dissolved portion participates in asphalt modification, forming DCLR-modified asphalt. Therefore, the dissolved portion of DCLR improves the performance of asphalt, increasing its adhesion and high-temperature resistance. On the other hand, the undissolved portion continues to function as particles, serving as fine

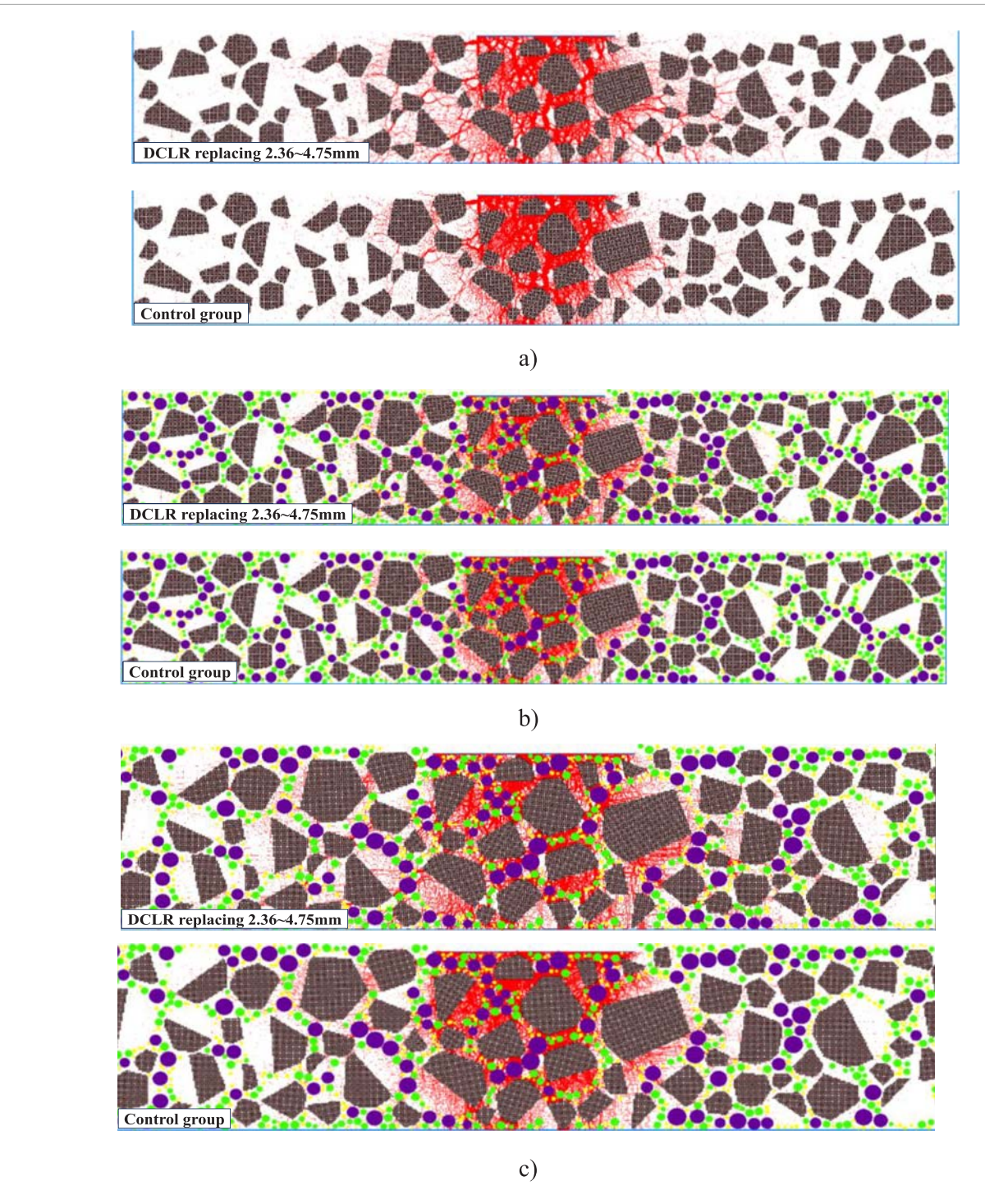
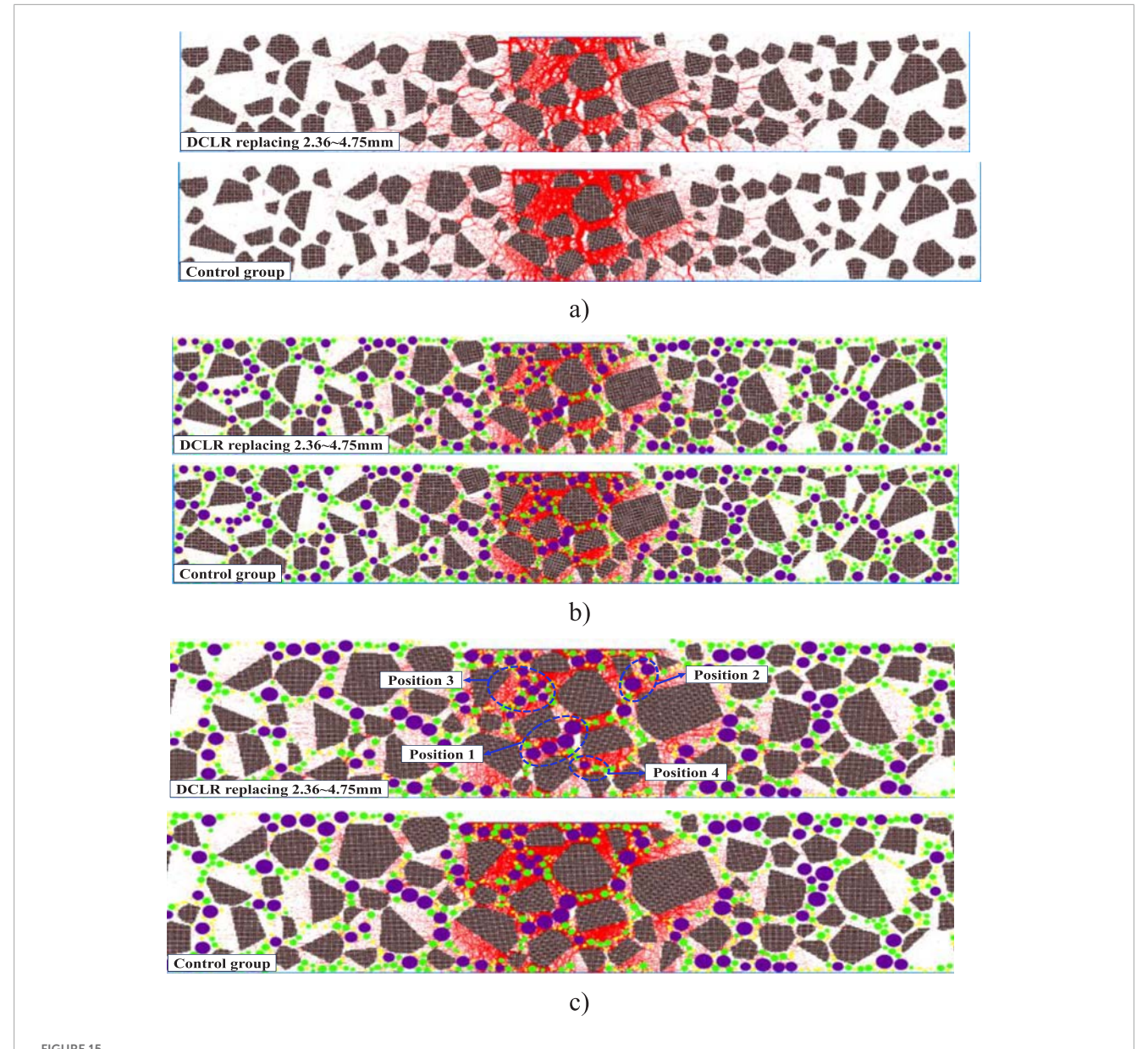


FIGURE 14
Enlarged diagram of force chain and aggregate distribution, and rutting formation position during the initial loading stage. (a) Force chain distribution.
(b) Aggregate distribution. (c) Enlarged view of the location of the rutting formation.

aggregate to fill gaps and forming a composite skeleton with coarse aggregate, thereby creating a new suspension-compacted structure. Therefore, when DCLR is added to asphalt mixtures as fine aggregate, it exhibits composite modification, combining the role of an asphalt modifier with the filling function of fine aggregate. That enhances

asphalt-aggregate bonding and improves particle connectivity, enabling better load redistribution across the entire model. Conversely, the control mixture's weaker particle correlations create stress concentration in wheel-track areas while leaving peripheral regions under-connected. These observations confirm DCLR's effectiveness in improving



Enlarged diagram of force chain and aggregate distribution and rutting formation position during loading. (a) Force chain distribution. (b) Aggregate distribution. (c) Enlarged view of the location of the rutting formation.

coordinated rut resistance throughout the asphalt mixture structure.

- 3. The force chain network exhibits a trapezoidal distribution, radiating from the model's top-center to its base and sides. Laterally, force chain intensity diminishes progressively from the wheel path (occupying one-third of the longitudinal dimension) toward the periphery. Vertically, chain density decreases significantly below two-thirds of the model height, becoming particularly sparse near the base. While 0.6–4.75 mm particles at the bottom periphery sustain minimal wheel loads, most sub-4.75 mm particles primarily function as fine aggregate fillers within the skeletal structure.
- 4. The magnified view reveals that initial loading is primarily borne by surface-layer components (0.6–4.75 mm fine aggregates and asphalt mortar) beneath the wheel, which subsequently transfer stress to coarse aggregates through mortar bonding. Force chains rapidly disperse across coarse aggregate surfaces (indicated by dense red spots denoting high stress), then propagate radially in dendritic patterns. Compared to SK-90 mixtures, coal liquefaction residue-modified mixtures exhibit smaller particle displacements and superior self-organization, resulting in sparser, more uniform force chain distributions that mitigate stress concentration in rutted areas.

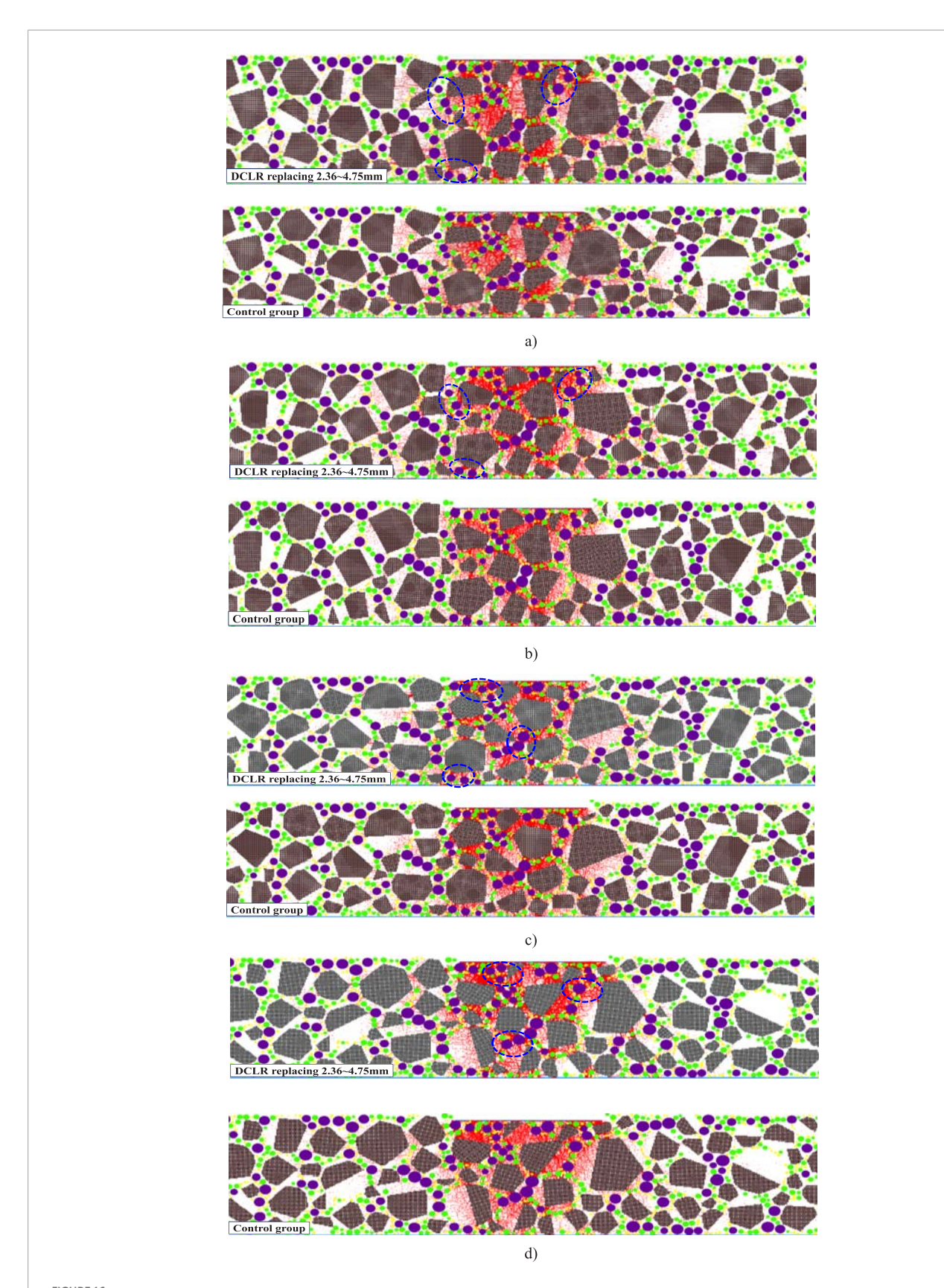


FIGURE 16
Force state of 2.36–4.75 mm particles under different clump coarse particle shapes. (a) Clump model one. (b) Clump model two. (c) Clump model three. (c) Clump model four.

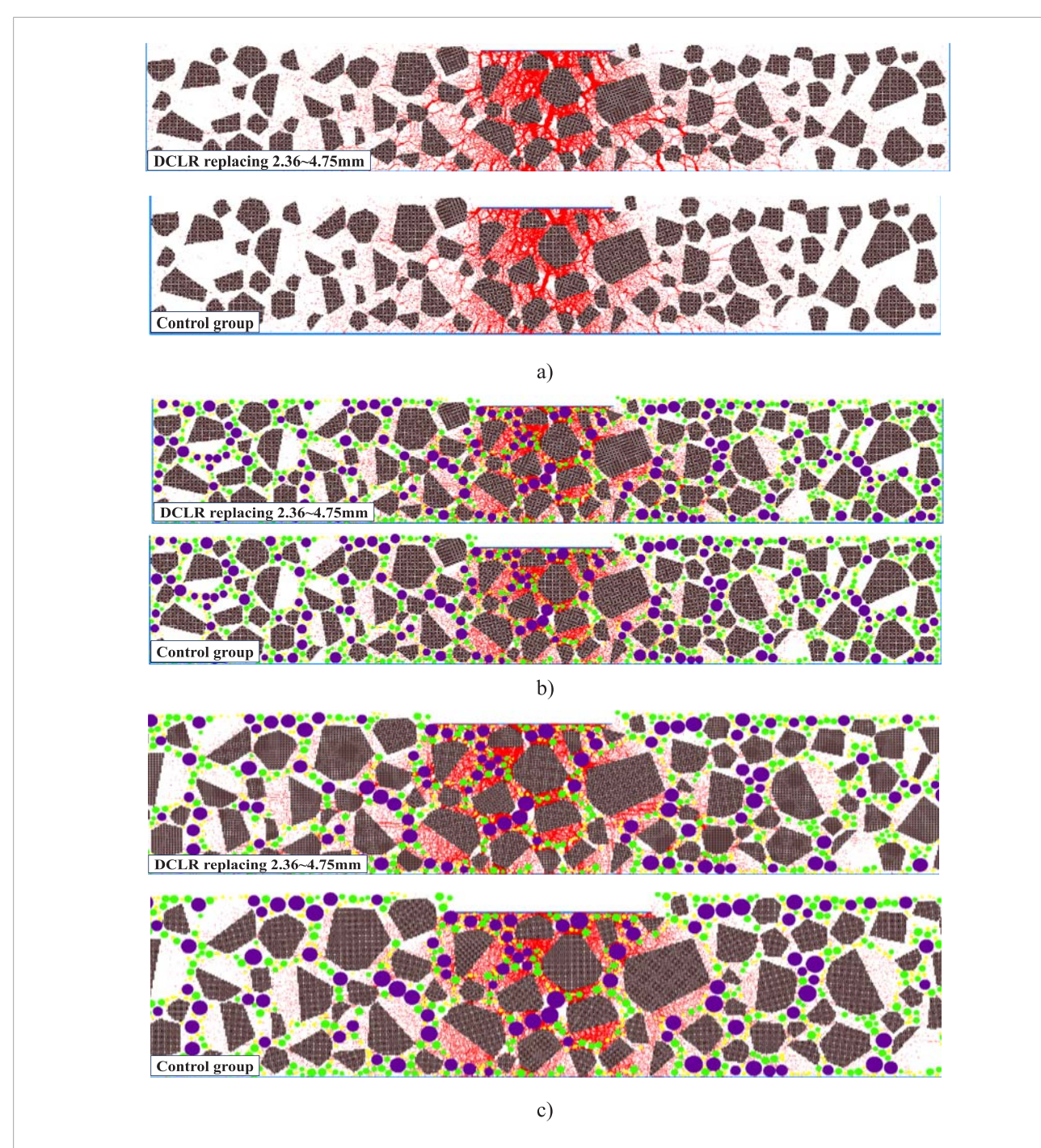


FIGURE 17
Enlarged diagram of force chain and aggregate distribution at the end of loading and the location of rutting formation. (a) Force chain distribution. (b)
Aggregate distribution. (c) Enlarged view of the location of rutting formation.

4.3.1.2 Load mid-term

Figure 15 shows the schematic diagram of the stress on DCLR single particle size replacement of $2.36-4.75~\mathrm{mm}$ fine aggregate and SK-90 asphalt mixture during the loading period of 20 min.

- Figure 15 demonstrates that load transmission occurs both vertically and laterally, radiating from contact points during loading. As rut depth increases in mid-stage loading, force
- distribution concentrates around protrusions. Vertically, force chain intensity peaks at two-thirds model height, with denser basal distribution compared to initial loading. Notably, bottom-layer particles progressively engage in load sharing, indicating enhanced stress redistribution.
- 2. While coarse aggregates form the primary skeleton in asphalt mixtures, force transfer between them occurs through

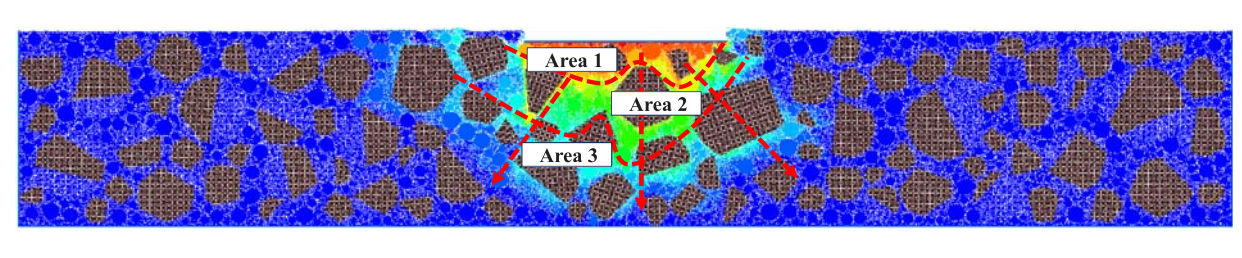


FIGURE 18
Displacement distribution.

fine aggregates. Mid-loading observations reveal dense red spots around aggregates, demonstrating how 2.36–4.75 mm DCLR particles (positions 1–2) effectively bridge coarse aggregates, exhibiting both macroscopic skeletal functions and microscopic force transmission capabilities. In contrast, smaller DCLR particles (0.6–2.36mm, positions 3–4) primarily serve as fillers with minimal contact force distribution. These findings highlight the dual structural role of 2.36–4.75 mm DCLR particles in maintaining both macro-scale framework stability and micro-scale force transmission.

To validate these findings and eliminate modeling randomness, we maintained constant particle counts per aggregate grade while randomly generating varied coarse aggregate shapes using Clump. Observations of 2.36–4.75 mm particle force distributions across different Clump configurations consistently confirmed the aforementioned analysis, as illustrated in Figure 16.

4.3.1.3 End of loading period

Figure 17 shows the schematic diagram of the stress of DCLR single particle size replacing 2.36 mm fine aggregate and SK-90 asphalt mixture at the end of 60 min of loading.

Figure 17 reveals that both control and experimental groups exhibited significant deformation in wheel-track areas by the loading period's end, showing both longitudinal and lateral displacement with distinct side protrusions. The applied load caused fine aggregates to detach from clumps, creating a denser, more uniform force chain network compared to earlier stages. Post-loading observations show complete separation of wheel-track fine aggregates from coarse aggregates, with 2.36–4.75 mm particles maintaining skeletal force transmission while 0.6–2.36 mm particles and asphalt mortar provide binding through coarse aggregate surface coating.

4.3.2 Correlation analysis between micro-force chain distribution and macro-rutting behavior

The evolution of the force chain network directly determines the macroscopic mechanical response of asphalt mixtures. During the initial loading stage (0–10 min), dense force chains concentrate beneath the wheel track, indicating local stress concentration and leading to rapid rutting formation. As loading time increases (10–20 min), the distribution of force chains in DCLR-modified mixtures becomes more uniform, reducing stress concentration and thereby delaying rut development. In the final stage (20–60 min), force chains redistribute in the peripheral regions of the wheel

track zone, forming stable load transfer paths that cause rut depth growth to plateau. This phenomenon indicates that the homogenization of micro-force chains is the key mechanism by which DCLR and ICLR enhance the anti-rut performance of the mixture, manifested macroscopically as the phased growth pattern of rut depth (Figures 6, 8) and a significant reduction in final deformation (Figure 5).

4.3.3 The influence of displacement distribution on rutting

The initial 20-min period represents the critical phase for rut formation in asphalt mixtures. Accordingly, our analysis focuses on displacement patterns during this timeframe, using the DCLR-modified mixture (2.36 mm replacement) as the representative case, as illustrated in Figure 18.

- Figure 18 reveals a characteristic "W"-shaped particle displacement pattern along the model's longitudinal axis under wheel loading. Particle movement occurs primarily along three distinct vectors: vertical, 45 ° left-diagonal, and 45 ° right-diagonal directions (as indicated by arrows), creating three distinct displacement zones corresponding to the "W" curve's segments.
- 2. The wheel-adjacent region shows particle displacement magnitude through orange color intensity, with 0.6–1.18 mm particles exhibiting the deepest hue (greatest displacement), followed by 1.18–2.36mm, while 2.36–4.75 mm particles show weaker (yellowish) displacement. This demonstrates that primary zone displacement results from direct force transmission, where larger particles absorb and redistribute forces through collisions, subsequently displacing smaller particles. Notably, displacement magnitude inversely correlates with particle size in this region, with finer particles experiencing greater movement.
- 3. The second region exhibits green-colored displacements, predominantly featuring 2.36–4.75 mm particles with relatively fewer 1.18–2.36 mm particles. Containing more clumps than the first region, displacement here primarily results from larger particles driving smaller ones through mechanical interaction.
- 4. The third region, located at the outer edges of the W-curve, predominantly contains 1.18–2.36 mm particles distributed sporadically along both sides. This zone features an intermediate clump concentration between the first and second regions. Analysis reveals that displaced particles

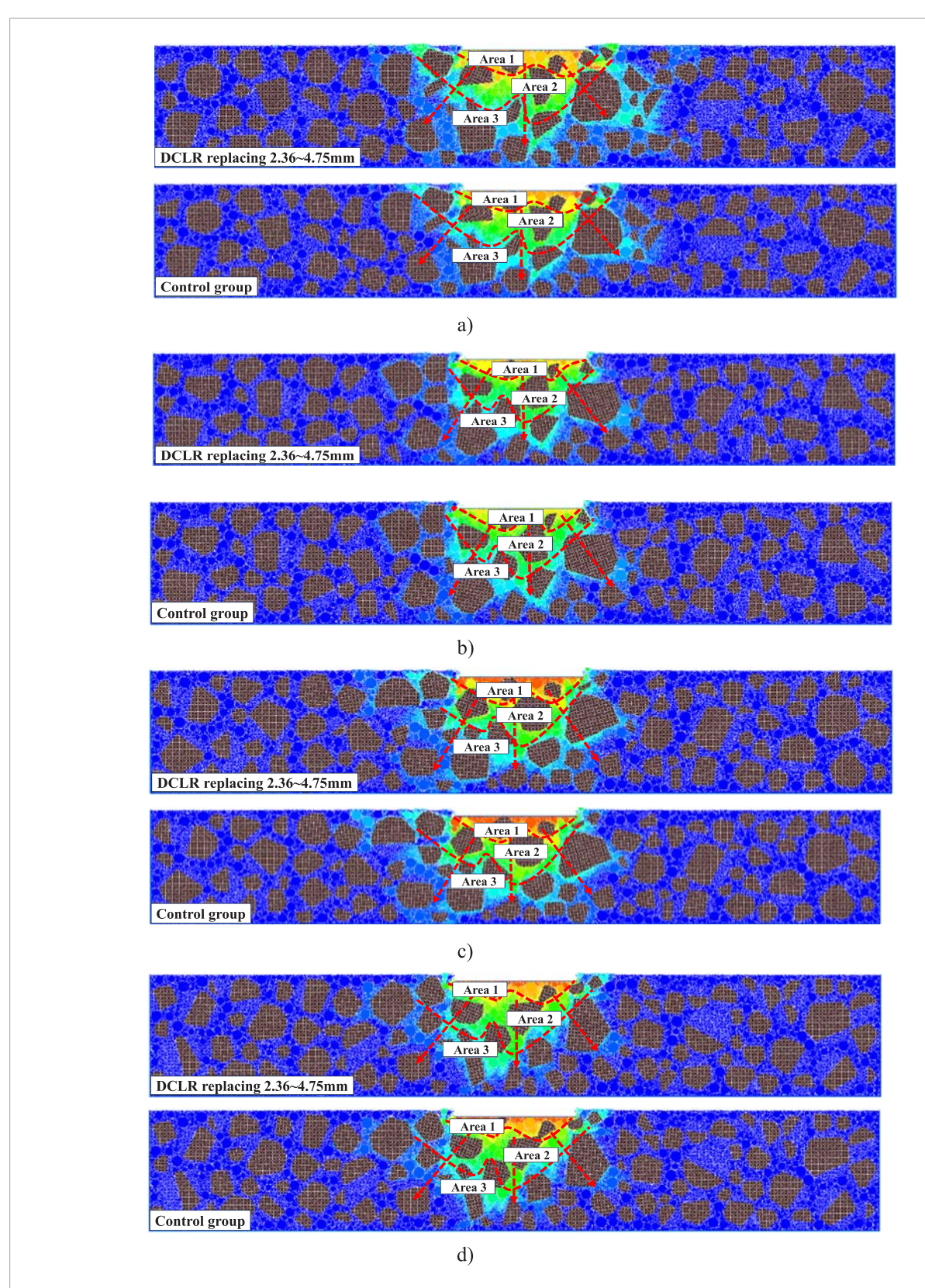


FIGURE 19
Displacement distribution under different clump coarse particle morphologies. (a) Clump model one. (b) Clump model two. (c) Clump model three. (d) Clump model four.

primarily concentrate within two-thirds of the vertical dimension and the longitudinal half-range centered on the wheel path.

To validate these findings and minimize modeling variability, consistent particle counts were maintained for each aggregate grade when generating random coarse aggregate configurations using Clump. Observations of 0.6–4.75 mm particle displacements across different zones confirmed consistency with our previous analysis, as demonstrated in Figure 19.

4.3.4 Correlation analysis between microscopic particle displacement and macroscopic rutting morphology

The spatiotemporal distribution characteristics of particle displacement are highly correlated with the macroscopic rutting morphology. Under wheel load, the significant displacement of fine particles (0.6-2.36 mm) (Figure 18) directly causes the "W"shaped subsidence in the central region of the wheel track zone (Figures 7, 9), while the skeletal role of particles (2.36-4.75 mm) restricts the expansion of lateral displacement, forming ridges on both sides (75-125 mm and 175-225 mm regions). In DCLRmodified mixtures, the displacement of fine particles is reduced due to enhanced asphalt adhesion (Figure 19), corresponding to a 33%-48% reduction in macro-scale rut depth (Figure 12). Additionally, the phased accumulation of displacement (rapid increase from 0 to 20 min, followed by stabilization from 20 to 60 min) aligns with the three-stage pattern of rut development (Figures 6, 8), confirming that micro-displacement mechanisms are the intrinsic driving force behind macro-rut evolution.

5 Conclusion

- 1. Temperature has a more significant impact on rutting behavior than mechanical loading. Rutting development follows a three-stage pattern: rapid growth (0–10 min), transitional phase (10–20 min), and stabilization (20–60 min), with the first 20 min being critical. The rut depth increases with temperature, showing a power-function relationship, while load increases cause smaller growth rates.
- 2. Rutting deformation primarily occurs in longitudinal zones of 75–125mm and 175–225 mm. ICLR substitution reduces rut depth by 19.69%–24.66% for 2.36–4.75 mm particles and 21.97%–22.94% for 1.18–2.36 mm particles, while DCLR shows superior performance with reductions of 33.73%–48.81%. The deformation patterns align with thermal-mechanical loading effects, with protrusion heights ranging from 0.5 to 4.2 mm.
- 3. The microstructure of coal liquefaction residue mixtures exhibits uniform force chain distributions, minimizing stress concentration. Smaller particles (0.6–2.36 mm) contribute more to deformation, while larger particles (2.36–4.75 mm) provide skeletal support and force transmission. Displacement is concentrated in the central two-thirds of the vertical zone and mid-longitudinal wheel path, with finer particles showing greater movement under load.
- 4. Optimal performance is achieved by replacing 1.18–2.36 mm particles with ICLR and 0.6–1.18 mm particles with DCLR.

DCLR outperforms ICLR due to its composite modification effect, enhancing adhesion and high-temperature resistance. Smaller DCLR particles (0.6 mm) form tighter bonds in asphalt mortar, reducing displacement, while ICLR's superior mechanical properties make it effective for 1.18 mm replacements. Both residues improve rutting resistance compared to conventional mixtures.

Data availability statement

The original contributions presented in the study are included in the article/supplementary material, further inquiries can be directed to the corresponding authors.

Author contributions

ZeW: Conceptualization, Methodology, Visualization, Writing - original draft. ZnW: Data curation, Formal Analysis, Writing - review and editing. CS: Funding acquisition, Writing - review and editing. SG: Funding acquisition, Investigation, Writing - review and editing. WZ: Resources, Software, Writing - review and editing. HC: Supervision, Validation, Writing - review and editing. XS: Resources, Supervision, Writing - review and editing. GC: Supervision, Validation, Writing - review and editing. PL: Methodology, Project administration, Writing - review and editing.

Funding

The author(s) declare that financial support was received for the research and/or publication of this article. This study is sponsored by the Nature Science Foundation of China of Jiangsu Province (NO. BK20230334), the National Nature Science Foundation of China (NSFC NO. 42407258), Natural Science Foundation of Chongqing (CSTB2025NSCQ-GPX0687; CSTB2024NSCQ-MSX1040). The Project of Construction and Support for high-level Innovative Teams of Beijing Municipal Institutions (BPHR20220109). The Cultivation project Funds for Beijing University of Civil Engineering and Architecture (X24013).

Acknowledgments

The authors appreciate all reviewers' constructive and helpful comments.

Conflict of interest

Authors ZeW, ZnW, CS, HC, and XS were employed by Beijing Municipal Road & Bridge Building Material Group Co. Ltd.

Author GC was employed by Qingdao NO1 Municipal Engineering Co., Ltd.

Author PL was employed by Beijing Xinqiao Technology Development Co., Ltd.

The remaining authors declare that the research was conducted in the absence of any commercial or financial relationships that could be construed as a potential conflict of interest. ensure accuracy, including review by the authors wherever possible. If you identify any issues, please contact us.

Generative AI statement

The author(s) declare that no Generative AI was used in the creation of this manuscript.

Any alternative text (alt text) provided alongside figures in this article has been generated by Frontiers with the support of artificial intelligence and reasonable efforts have been made to

Publisher's note

All claims expressed in this article are solely those of the authors and do not necessarily represent those of their affiliated organizations, or those of the publisher, the editors and the reviewers. Any product that may be evaluated in this article, or claim that may be made by its manufacturer, is not guaranteed or endorsed by the publisher.

References

Chen, L. (2019). Research on anti-rutting performance of direct coal liquefaction residue modified asphalt mixture (in Chinese). Beijing: Beijing University of Civil Engineering and Architecture.

Fan, Y. (2011). An exploratory study on the nature and application of coal direct liquefaction residue [D]. Shanghai: East China University of Science and Technology.

Fan, B. (2014). Experimental study on viscoelastic plastic constitutive model and long-term creep behavior of asphalt mixture. Hubei, Wuhan: Huazhong University of Science and Technology.

Gao, H. U. (2018). DEM simulations and study of fracture and rutting behaviors for asphalt mixture. Hubei, Wuhan: Huazhong University of Science and Technology.

Gu, X., Zhou, M., and Shi, S. (2006). Molecular structure of heavy oil fraction from the Shenhua coal direct liquefaction residue. *J. China Coal Soc.* (1), 76–80.

He, L. (2013). Study on the preparation and performance of asphalt modified by Coal liquefaction residue[D]. Shaanxi, Xi'an: Chang'an University.

Hu, M., Lihan, Li, Wang, J., and Yang, K. (2019). Experimental study on pavement performance and leaching characteristic of asphalt mixture with bottom ash aggregate. *J. Build. Mater.* 22 (3), 480–486.

Ji, J., Shi, Y., Suo, Z., Yao, H., and Shifa, Xu (2015). Influence of direct coal liquefaction residue on viscoelastic properties of asphalt mortar. *J. Traffic Transp. Eng.* 15 (4), 1–8.

Ji, J., Yao, H., Wang, Di, Suo, Z., Liu, L., and Zhanping, Y. (2017). Properties of direct coal liquefaction residue modified asphalt mixture. *Adv. Mater. Sci. Eng.* 2017, 1–11. doi:10.1155/2017/2473283

Ji, J., Ma, R., Zheng, W., Suo, Z., and Ying, Xu (2018). Effect of DCLR and TLA on adhesion characteristics of asphalt and aggregate (in Chinese). *J. Chongqing Jiaot. Univ. Nat. Sci.* 37 (1), 54–61.

Ji, J., Chen, L., Suo, Z., Ying, Xu, and Han, Y. (2019). Effect of high temperature and heavy load on deformation resistance of DCLR modified asphalt mixture (in Chinese). *J. Traffic Transp. Eng.* 19 (1), 1–8.

Ji, J., Hui, Li, Ying, Xu, Shi, Y., and Zhi, S. (2019a). Rheological properties of asphalt binder modified by tetrahydrofuran soluble extracted from direct coal liquefaction residue. *J. Chang'an Univ. Nat. Sci. Ed.* 39 (4), 9–16.

Ji, J., Wang, Z., Zhang, R., Jianming, W., Suo, Z., Zhanping, Y., et al. (2020). Rutting resistance of direct coal liquefaction residue (DCLR) modified asphalt mixture under variable loads over a wide temperature range. *Constr. Build. Mater.* 257, 119489. doi:10.1016/j.conbuildmat.2020.119489

Ji, J., Chen, M., Suo, Z., Jianming, W., Wang, J., and Chen, L. (2021). Rutting prediction model of asphalt mixture based on the triaxial Repeated load test. *Adv. Civ. Eng.* 2021, 5238680–5238689. doi:10.1155/2021/5238680

Ji, J., Wang, Z., Pengfei, Li, Zheng, W., Xinqiang, Xu, Wang, Z., et al. (2023). A review on direct coal liquefaction residue applied in asphalt pavements. *J. Clean. Prod.* 395, 136273. doi:10.1016/j.jclepro.2023.136273

Lin, Q., Jianghua, Li, Yaozu, Ma, and Qiang, Y. (2018). Study on the influence of blast furnace slag as aggregate on low-temperature performance of asphalt road (in Chinese). West. China Commun. Sci. & Technol. (8), 18–21.

Liu, W., Mao, H., Mao, H., and Ruixia, Li (2021). Study on the effect of coal oil residue on high temperature-fatigue rheological properties of asphalt binder (in Chinese). *Highw. Eng.* 46 (1), 73–80.

Liu, D., Lihan, Li, and Cui, H. (2015). Experimental study on influence of municipal solid waste incineration bottom ash aggregate on properties of asphalt mixture. *J. Build. Mater.* 18 (2), 307–311.

Liu, Z., Sun, Y., Weihua, L. I., Yang, Q., and Qiang, M. A. (2016). Research progress of gasification slag utilization from indirect coal liquefaction process. *Clean. coal Technol.* 22 (1), 118–123.

Mingfeng, C., Pei, J., Huang, P., and Rui, X. (2018). Analysis on the distribution Probability of force chain of contact force among granular matter considering gradation. 32(20):3618–3622.

Ministry of Transport of the People's Republic (2011). Standard test methods of bituminous mixture for highway engineering (JTG E20-2011). Beijing, China: Renmin Communication Press. (in Chinese).

Peng, T. (2016). Discrete element method simulation of rutting deformation of asphalt mixture. Hubei, Wuhan: Huazhong University of Science and Technology.

Ren, Z. (2020). Research on composition design and performance of asphalt mixture with coal gasification fine slag blended by salt (in Chinese). Shaanxi, Xi'an: Chang'an University.

Rondon-Quintana Hugo, A., Ruge-Cardenas Juan, C., Patino-Sanchez Daniel, F., Vacca-Gamez Hermes, A., Reyes-Lizcano Fredy, A., and Muniz, de F. M. (2018). Blast furnace slag as a substitute for the fine fraction of aggregates in an asphalt mixture. *J. Mater. Civ. Eng.* 30 (10), 4018244.

Rong, L., Yuan, Xu, Liu, H., and Zhang, D. (2018a). GuangleRheological mechanical properties of DCLR-modified asphalt binders (in Chinese). *China J. Highw. Transp.* 31 (6), 165–171.

Rong, L., Yuan, Xu, Liu, H., Zhang, D., and Guangle, F. (2018b). Rheological mechanical properties of DCLR-modified asphalt binders. *China J. Highw. Transp.* 31 (6), 165–171.

Shi, yuefeng (2017). Research on preparation and performances of direct coal liquefaction residue modified asphalt (in Chinese). Beijing: Beijing University of Civil Engineering and Architecture.

Wang, H., Zhou, C., and Chen, Q. (2015). Impact of coal cinder content on mechanical properties of ash residue mixture (in Chinese). *Water Resour. Power* 33 (9), 113–116

Wang, X., Hu, F., and Wang, G. (2020). Research status and prospect of coal indirect liquefaction synthetic oil technology. *Clean. coal Technol.* 26 (1), 110–120.

Wang, B., Lu, Li, Yujiao, X., Yu, P., and Wenchao, H. (2022a). Fundamental coal demand prediction under the goal of carbon neutrality in 2060. *Clean. coal Technol.* 28 (5), 1–13.

Wang, S., Liu, F., Xiao, Z., Gao, Y., Kong, Q., and Liu, X. (2022b). Study on the effect of coal gasification slag on rheological properties of asphalt mastic. *J. Funct. Mater.* 53 (6), 6025–6034.

Wang, Z., Ji, J., Han, B., Li, P., Wang, Z., and Li, H. (2022c). Laboratory investigation on pavement performance of indirect coal liquefaction residue in asphalt mixture. *J. Clean. Prod.* 363, 132183. doi:10.1016/j.jclepro.2022.132183

Wu, H. (2019). Study on compatibility between direct coal liquefaction residue and bitumen (in Chinese). Beijing: Beijing University of Civil Engineering and Architecture.

Zhai, X., Chen, Bo, and Ding, L. (2019). Influence of ZnO on anti-permanent deformation and anti-UV ageing performances of DCLR modified asphalt (in Chinese). Highw. Eng. 44 (4), 74–78.

Zhang, Y. (2021). Study on process and property of modification of petroleum asphalt with direct coal liquefaction residue (in Chinese). Shanxi, Taiyuan: Taiyuan University of Science and Technology.

Zhang, Y. L., Chen, Y., Chen, Li, Wang, J., Dong, F., and Chuang, G. (2018). Performance of coal liquefied residue asphalt stabilized gravel base materials with dry mixing method (in Chinese). *J. Chongqing Jiaot. Univ. Nat. Sci.* 37 (11), 47-51

Zhi, S., Jie, Ji, Ran, Z., Wang, Z., Yao, H., and Jin, D. (2020). Effects of tire pressures and test temperatures on permanent deformation of direct coal liquefaction residue (DCLR) mixture. Front. Matrerials 7 (246), 1-9.